ChemComm

REVIEW ARTICLE

View Article Online
View Journal | View Issue

Cite this: *Chem. Commun.*, 2026, **62**, 6503

A biocatalytic reticular framework *via* enzyme immobilization for environmental pollutant monitoring

Rui Gao,[a] Xiaoxue Kou,[b] Jing Li,*[c] Siming Huang,[d] Jiehao Yu,[e] Zhi-Wei Li,*[e] Guosheng Chen[b] and Gangfeng Ouyang[b]

The growing prevalence of anthropogenic pollutants demands the advancement of environmental monitoring technologies. Biocatalytic sensing, leveraging enzymatic specificity and efficiency, offers a promising alternative, yet the structural fragility and instability of free enzymes limit its practical application. A transformative strategy involves immobilizing enzymes within engineered porous frameworks, such as metal–organic frameworks (MOFs) and covalent organic frameworks (COFs). These crystalline materials offer ultrahigh surface areas, tunable pore structures, and versatile surface chemistry, forming an ideal platform for constructing robust biohybrid sensing systems. They not only enable high enzyme loading but also establish a stabilized microenvironment that enhances enzymatic activity, stability, and reusability, while significantly improving catalytic selectivity and sensitivity. This review explores the strategic integration of enzymes with porous frameworks, detailing immobilization methodologies toward biosensing platforms. By examining their application in detecting pesticides, phenolic compounds, antibiotics, pathogens, and emerging contaminants, we highlight their potential to revolutionize environmental monitoring. Finally, we discuss current challenges and outline future directions to guide the development of sensitive, durable, and field-deployable analytical systems for sustainable environmental stewardship.

Received 13th December 2025,
Accepted 3rd March 2026

DOI: 10.1039/d5cc07082a

rsc.li/chemcomm

[a] *Institute for Advanced Study, Chengdu University, Chengdu 610106, People's Republic of China*
[b] *MOE Key Laboratory of Bioinorganic and Synthetic Chemistry, School of Chemistry, Sun Yat-sen University, Guangzhou 510275, People's Republic of China*
[c] *College of Food and Biological Engineering, Chengdu University, Chengdu 610106, People's Republic of China. E-mail: lijing@cdu.edu.cn*
[d] *Guangzhou Municipal and Guangzhou Province Key Laboratory of Molecular Target & Clinical Phamacology, the NMPA and State Key Laboratory of Respiratory Disease, School of Phamaceutical Sciences and the Fifth Affiliated Hospital, Guangzhou Medical University, Guangzhou 511436, People's Republic of China*
[e] *College of Chemistry and Materials, Jiangxi Normal University, Nanchang 330022, People's Republic of China. E-mail: lizhw69@mail.sysu.edu.cn*

Rui Gao

Rui Gao is an assistant researcher at the Institute for Advanced Study, Chengdu University, China. He received his PhD degree in Environmental Chemistry from Sun Yat-sen University, Guangzhou, China. He worked as a postdoc from 2022 to 2024 at Sun Yat-sen University with Prof. Gangfeng Ouyang. His research focuses on the development of protein–porous organic framework biocomposites and their application in environmental analysis and remediation.

Xiaoxue Kou

Xiaoxue Kou received her master's degree in Environmental Chemistry from Sun Yat-sen University in 2021. She is now a doctoral student at Sun Yat-sen University. Her current research focuses on engineering porous organic frameworks as nanozymes for biocatalysis and biosensing.

1. Introduction

The escalating release of environmental pollutants, fueled by rapid industrialization, population growth, and unsustainable production, has intensified ecological crises worldwide.[1,2] The widespread use of pesticides,[3] phenolics,[4] and antibiotics,[5] and emerging biological contaminants like pathogenic bacteria[6] have contributed to pervasive environmental contamination. Regulatory mandates, such as those from the U.S. EPA, establish stringent maximum contaminant levels, necessitating the development of analytical methods capable of reliable, sensitive, and selective detection at trace concentrations (ppb to ppt) of pollutants in intricate matrices like wastewater, soil, and biological fluids.[7] This scenario presents a quintessential analytical challenge, where achieving accurate quantification requires overcoming significant and variable background interference through exceptional selectivity and sensitivity.

While conventional laboratory techniques such as chromatography coupled with mass spectrometry remain the gold standard for confirmatory multi-residue analysis due to their high accuracy, they are often limited by operational complexity, high cost, and poor suitability for real-time, on-site monitoring.[8] Consequently, the field is increasingly shifting toward biosensing platforms that offer the potential

Jing Li

Jing Li is an associate professor of applied chemistry at the College of Food and Biological Engineering, Chengdu University, China. She received her PhD in Analytical Chemistry from Sichuan University in 2014 under the supervision of Prof. Dan Xiao. She was a winner of the Natural Science Foundation of Sichuan Province. Currently, her research is focused on the fundamental research on electrochemical sensors and the design of new functional materials for food and environmental analyses.

Siming Huang

Siming Huang is a professor at the School of Pharmaceutical Sciences, Guangzhou Medical University, China. She received her BSc degree in chemistry from Sun Yat-sen University, Guangzhou, China, in 2013, and her PhD in Physical Chemistry from the same university in 2018 under the supervision of Prof. Gangfeng Ouyang. She worked as a postdoc from 2019 to 2020 at Sun Yat-sen Memorial Hospital, Guangzhou, China. She has published more than 40 peer-reviewed publications in Chem, Angew. Chem., Nat. Commun., etc. Her current research is focused on the design of functional nanomaterials for cancer therapy and detection of disease biomarkers.

Jiehao Yu

Jiehao Yu received his master's degree in chemistry from East China University of Technology in 2020. He is now a doctoral student at the College of Chemistry and Materials Science, Jiangxi Normal University, China. His current research focuses on supramolecular chemistry and dynamic self-assembly.

Zhi-Wei Li

Zhi-Wei Li is a lecturer in chemistry at the College of Chemistry and Materials Science, Jiangxi Normal University, China. He received his BE degree in Polymer Materials and Engineering in 2015 and his PhD degree in Inorganic Chemistry in 2020, both from Sun Yat-sen University (SYSU), China. From 2020 to 2024, he conducted postdoctoral research at the School of Chemistry, SYSU, under the supervision of Professor Gangfeng Ouyang. In 2025, he joined Jiangxi Normal University as a faculty member in Professor Xiaoyu Hu's research group. His current research is focused on the design and application of supramolecular compounds, including macrocycles, hydrogen-bonded organic frameworks (HOFs), and covalent organic frameworks (COFs), with an emphasis on small molecule activation and environmental analysis.

for decentralized, rapid, and cost-effective environmental monitoring.

Enzyme-based biosensors represent a particularly promising alternative, leveraging the innate catalytic efficiency and molecular recognition specificity of enzymes, described as a "lock-and-key" mechanism, to achieve high selectivity even in complex sample environments.[9–11] Their operation under mild, aqueous conditions further aligns with the principles of green analytical chemistry.[12] However, the widespread deployment of native enzymes is significantly hampered by their intrinsic structural instability. Enzymes are conformationally labile biomacromolecules, and hence their catalytic activities are readily disrupted by non-physiological conditions commonly encountered in environmental samples, including extreme pH, temperature fluctuations, organic solvents, and chemical denaturants.[13,14] This instability leads to signal drift, reduced shelf-life, and poor batch-to-batch reproducibility, compromising the accuracy, long-term reliability, and cost-effectiveness of the sensor, posing a major barrier to their real-world application.

Recent developments in enzyme immobilization have employed various nano- and microstructured carriers to improve enzymatic stability through spatial confinement, such as carbon-based materials, polymeric matrices, and porous nanoparticles.[15–17] However, conventional supports often exhibit limited enzyme loading capacity and constrained pore accessibility, which consequently reduce catalytic efficiency. A transformative alternative has emerged with the use of porous reticular frameworks, including metal–organic frameworks (MOFs) and covalent organic frameworks (COFs).[18–20] These materials offer an ideal platform for enzyme immobilization due to their high surface area, tunable porosity, and structural robustness.[3,12,21–27] From an analytical standpoint, these frameworks deliver multiple critical advantages. First, the rigid porous architecture functions as a protective "exoskeleton" that confines enzymes and mitigates denaturation, thereby extending operational half-life and enhancing reusability. This directly translates into biosensors with improved durability, reproducibility, and cost-effectiveness.[21,22] Second, well-defined mesopores facilitate efficient mass transfer of substrates and products, minimizing diffusion limitations that typically suppress apparent activity in conventional immobilized systems. As a result, catalytic turnover rates are maintained or even amplified, leading to stronger signal output and higher sensitivity. Moreover, the tailored pore dimensions can act as molecular sieves, selectively excluding interfering species from reaching the enzymatic active site.[28,29] This "gatekeeping" function significantly enhances selectivity by reducing nonspecific interactions and background noise. Collectively, these attributes enable the design of robust, portable, and reusable biosensors suitable for decentralized, real-time environmental monitoring.

This review systematically summarizes recent advances in the rational design of biocatalytic reticular framework hybrids *via* enzyme immobilization for environmental sensing. We critically analyze key developments in functional integration strategies, such as surface adsorption, surface covalent anchoring, pore entrapment, and *in situ* encapsulation, and evaluate their impact on catalytic performance and operational stability. These engineered hybrids enable the highly sensitive and selective detection of a broad spectrum of environmental pollutants, including pesticides, antibiotics, phenolic compounds, and pathogenic microorganisms. Furthermore, the review identifies current limitations and outlines promising research directions aimed at enhancing real-world applicability. By integrating perspectives from materials science, analytical chemistry and environmental engineering, we provide a cross-disciplinary foundation for the next generation of smart, field-deployable biosensors.

Guosheng Chen

Guosheng Chen is an associate professor of chemistry at the School of Chemistry, Sun Yat-sen University, China. He received his BSc degree in Applied Chemistry from Sun Yat-sen University, Guangzhou, China in 2013 and then received his PhD Degree in Physical Chemistry from the same university in 2018 under the supervision of Prof. Gangfeng Ouyang. He worked as a postdoc from 2019 to 2020 at Sun Yat-sen University. He has published more than 60 peer-reviewed publications in Chem, Nat. Commun., Angew. Chem., Int. Ed., Chem. Sci., Adv. Funct. Mater., etc. His research interests include engineering biofunctional nanomaterials, particularly protein–porous organic framework biocomposites, and their application in biosensing, catalytic therapy and nanomotors.

Gangfeng Ouyang

Gangfeng Ouyang is a professor of chemistry at the School of Chemistry, Sun Yat-sen University, China. He received his PhD in Physical Chemistry from Sun Yat-sen University in 2003 under the supervision of Prof. Beisheng Kang. He worked as a postdoc at the University of Waterloo, Canada, in the group of Prof. Janusz Pawliszyn. He was a winner of the National Science Fund for Distinguished Young Scholars and Distinguished Professor of "Zhujiang Scholar". Currently, his research is focused on the fundamentals of microextraction technology and the design of new functional materials for biocatalysis, photocatalysis and environmental analysis.

2. Enzyme immobilization strategies

The enzyme immobilization strategies are broadly classified into two categories based on the enzyme's localization relative to the framework structure. This section will provide a concise overview of the distinct immobilization principles and their individual characteristics (Fig. 1).

2.1. Enzyme-on-porous reticular frameworks

Porous reticular frameworks, characterized by their tunable surface physicochemical properties and engineered functional groups, offer abundant binding sites for the surface bioconjugation of enzymes through supramolecular interactions. This approach demonstrates broad applicability and eliminates size constraints on the anchored biomolecules. In addition, it preserves the activity of the surface-immobilized enzymes due to minimal structural perturbation from the supporting matrix and optimal exposure to the surrounding microenvironment. This bioconjugation strategy primarily encompasses two mechanisms: surface adsorption *via* noncovalent interactions and covalent anchoring.

2.1.1. Surface adsorption *via* noncovalent interactions. Surface adsorption *via* noncovalent interactions serves as a straightforward and versatile strategy for enzyme immobilization, wherein enzymes are non-covalently anchored onto pre-synthesized reticular architectures through weak intermolecular interactions such as van der Waals forces, hydrogen bonding, π–π stacking, hydrophobic effects, and electrostatic complementarity.[22,30] This methodology is characterized by operational simplicity and mild implementation conditions.[31] A representative example is the work by Ma *et al.*[32] who developed a surface-modified adsorption strategy for immobilizing pepsin (PEP) on ZIF-8. They first electrostatically coordinated Ni^{2+} with the electronegative ZIF-8, which effectively modulated the inherent hydrophobicity of the material. The immobilized Ni^{2+} ions then served as anchoring sites for PEP *via* favorable electrostatic attraction (Fig. 2a). This physical adsorption method is not only operationally simple and adaptable to various enzymes but also typically preserves high enzymatic activity upon immobilization, as the weak interactions minimize structural disruption of the enzyme.

From the standpoint of analytical performance, the retained activity, attributed to favorable enzyme orientation and reduced diffusion limitations for substrates, directly contributes to amplified signal generation, thereby lowering the limit of detection for target analytes and improving assay sensitivity. Nevertheless, the stability and reproducibility of such systems remain challenging under dynamic operational conditions. As mentioned earlier, environmental factors such as pH fluctuations and variations in ionic strength can dynamically perturb the adsorption equilibrium, potentially leading to substantial enzyme leaching over time. This desorption behavior poses a significant limitation for long-term or field applications.

2.1.2. Surface covalent anchoring. Surface covalent anchoring overcomes the limitations of adsorption-based methods by forming chemically stable bonds between the functional groups on the support material and the reactive residues on the biomacromolecules, thereby ensuring robust and durable immobilization to prevent the leaching issue. Common functional moieties such as carboxyl, azide, and epoxy groups enable site-specific conjugation with complementary groups (*e.g.*, amino, carboxyl, or thiol) on enzyme surfaces.[33] For instance, Lu *et al.*[34] immobilized glucose oxidase (GOx) onto an epoxy-functionalized COF *via* covalent bonding (Fig. 2b). This approach increased the enzyme loading from 26 mg g^{-1} (by physical adsorption) to 40 mg g^{-1}. In reuse stability tests, the covalently immobilized enzyme retained over 95% of its initial activity after six cycles, significantly outperforming the

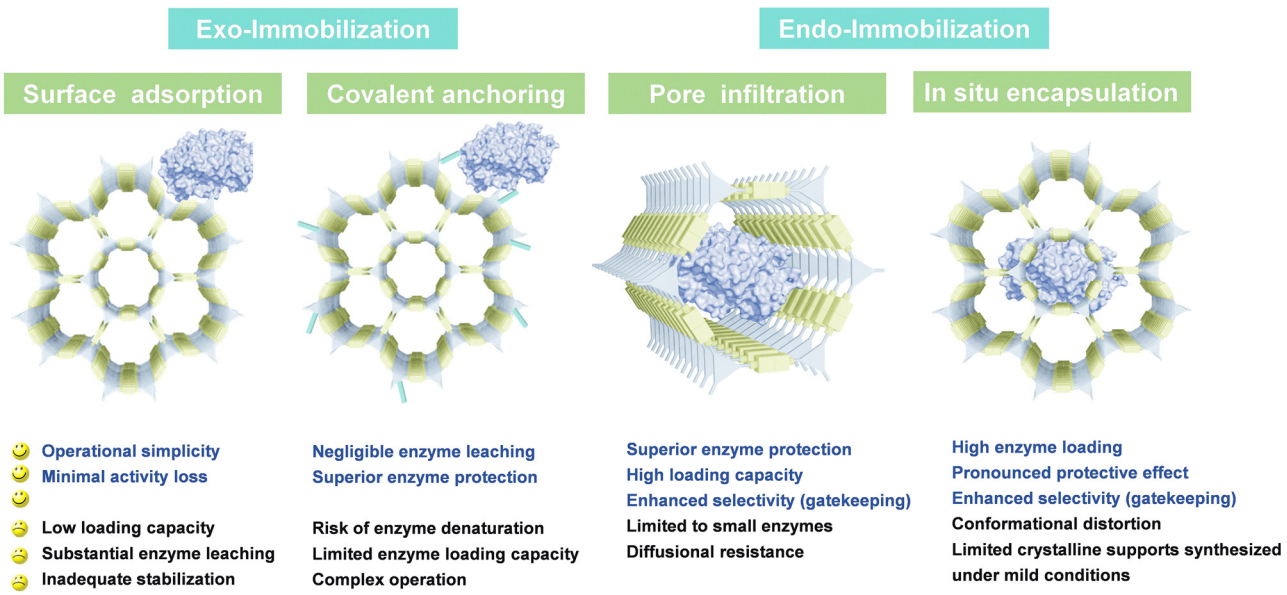

Fig. 1 Schematic illustration of immobilization types of enzyme–porous reticular framework hybrids and their individual characteristics.

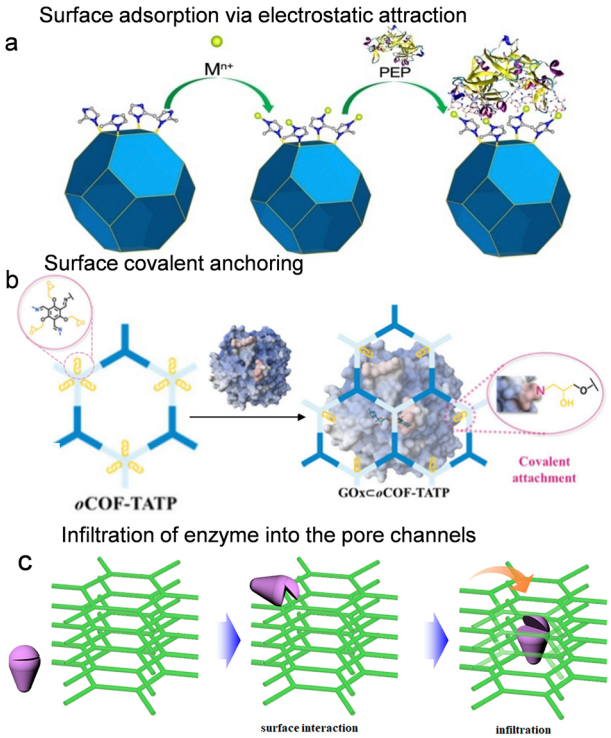

Fig. 2 Enzyme immobilization on/into porous reticular frameworks *via* surface attachment and pore encapsulation methods. (a) Schematic illustration of surface adsorption *via* electrostatic attraction interactions of PEP to ZIF-8, reproduced from ref. 32 with permission from Wiley, *Angew. Chem., Int. Ed.*, 2023, **62**, e202216699, copyright 2023. (b) Covalent conjugation of glucose oxidase to COF carriers through surface-grafted epoxy groups, reproduced from ref. 34 with permission from American Chemical Society, *Langmuir*, 2025, **41**, 11765–11775, copyright 2025. (c) Schematic illustration of the translocation of the enzyme into the pore channels, reproduced from ref. 35 with permission from American Chemical Society, *J. Am. Chem. Soc.*, 2018, **140**, 984–992, copyright 2018.

physically adsorbed system, which retained only 65.1% activity due to substantial enzyme leakage. Despite these advantages, covalent immobilization presents several challenges. A significant fraction of enzymes remains directly exposed to the external environment, making them susceptible to denaturation under external stimuli. Moreover, immobilization tends to occur predominantly on the outer surface of the framework, underutilizing the internal porous architecture and limiting enzyme loading capacity. Consequently, although covalent anchoring improves operational stability, it may only partially preserve the enzyme's native conformation and often leads to suboptimal immobilization efficiency, thereby reducing specific activity and compromising selectivity.

2.2. Enzyme-in-porous reticular frameworks

This approach involves the encapsulation of enzymes within the nanopores or defective cavities of crystalline frameworks, fully leveraging the host architecture to provide physical protection and enhance biocatalyst stability under operational stressors.

2.2.1. Pore encapsulation. This strategy entails the infiltration and entrapment of enzyme molecules within the pre-synthesized pores of a framework, typically *via* diffusion from solution.[36] As a post-synthetic process conducted under mild conditions, it avoids chemical modification of the enzyme, thereby preserving its native structure and activity. Successful encapsulation critically depends on size matching between the enzyme and the pores of the framework, in which the pore apertures must be sufficiently large to permit enzyme entry.[37] Consequently, this method is generally applicable to mesoporous frameworks (pore diameters $>$ 2 nm) for most enzymes. In a pioneering study, Ma *et al.*[38] encapsulated microperoxidase-11 (MP-11) within a terbium-based mesoporous MOF (Tb-mesoMOF). The resulting MP-11@Tb-mesoMOF composite exhibited higher enzyme loading and catalytic activity than MP-11 supported on mesoporous silica, along with improved cycling stability and solvent compatibility, enabling efficient oxidation catalysis even in organic media. Similarly, the tunable pore environments of COFs offer opportunities to enhance enzymatic performance. For example, lipase PS was encapsulated in COF-OMe, which possesses ordered one-dimensional channels (3.3 nm). Compared to solid supports with similar pore sizes, such as hierarchically porous MOF PCN-128y and mesoporous silica MCM-41, COF-OMe showed higher enzyme loading and superior catalytic performance. Importantly, the activity of the encapsulated lipase PS varied with the functionalization of the pore walls, highlighting how programmable host–guest interactions can be tailored to optimize enzyme function.[35] To address mass transport limitations, hierarchical porous frameworks have been developed. Farha and colleagues, for instance, designed a series of zirconium-based MOFs (NU-100x, x = 3–7) with interconnected meso-/macropores, where larger pores host bulky enzymes while smaller channels facilitate efficient diffusion of substrates and products.[39] Additionally, hierarchical porous COFs featuring two types of pores have been shown to promote enzyme encapsulation efficiency and activity. Furthermore, the adjustable pore structure provides favorable microenvironments, resulting in activating enzymes through the complicated interface process between the enzyme and the pore wall.[40] Such biohybrid systems not only exhibit excellent long-term performance under aqueous conditions but also demonstrate enhanced stability in complex matrices. In addition, the precisely tailored pore dimensions can function as ''gatekeepers'', selectively excluding interfering species from accessing the enzymatic active site, thereby significantly enhancing assay selectivity.[29] However, the prerequisite for precise pore size matching inherently restricts this strategy to biomolecules smaller than the host pore dimensions. Moreover, the synthesis of mesoporous and macroporous frameworks typically involves multistep and intricate procedures, which may pose challenges for large-scale production and practical deployment.

2.2.2. *In situ* encapsulation. *In situ* encapsulation involves the direct incorporation of enzymes into a porous crystalline matrix during its formation. In this approach, framework precursors (*e.g.*, metal ions and organic linkers) co-assemble

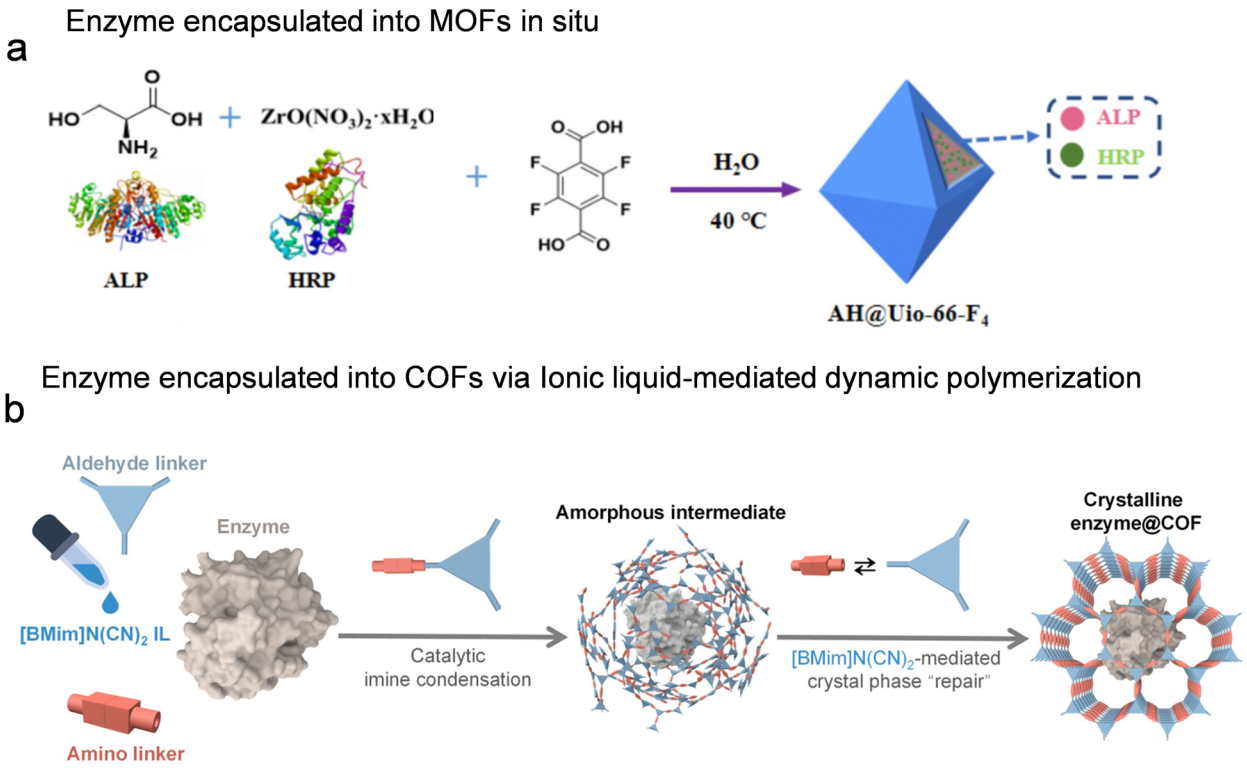

Fig. 3 *In situ* encapsulation of enzyme in porous reticular frameworks. (a) Preparation of AH@UiO-66-F_4 *in situ*, reproduced from ref. 42 with permission from Elsevier, *Food Chem.*, 2025, **493**, 145602, copyright 2025. (b) Ionic liquid-mediated dynamic polymerization of COF, reproduced from ref. 29 with permission from Wiley, *Angew. Chem., Int. Ed.*, 2024, **63**, e202319876, copyright 2024.

with enzymes in solution, leading to crystallization of the framework around the enzyme molecules. This process entraps the enzymes within the growing crystal lattice, forming a rigid and protective shell that minimizes enzyme leaching and enhances stability under harsh environmental conditions. Moreover, this encapsulation strategy also preserves the "gatekeeping" function of the porous framework, which significantly enhances assay selectivity by excluding interfering species and reducing nonspecific background signals. Importantly, this strategy enables the encapsulation of enzymes larger than the intrinsic pore dimensions of the mature framework and often achieves high enzyme loading while preserving bioactivity.[41–43]

2.2.2.1. MOFs. ZIF-8 is widely used for enzyme encapsulation owing to its mild synthesis conditions (*e.g.*, room temperature operation in aqueous media). It has been successfully applied to immobilize a variety of enzymes, including laccase (LAC),[44] horseradish peroxidase (HRP),[45] cytochrome *c* (Cyt *c*),[46] acetylcholinesterase (AChE),[47–49] and herbicide hydrolase.[50] The resulting ZIF-8-enzyme composites have shown significant potential in the detection of pesticides and phenolic compounds, with the framework enhancing enzymatic stability under challenging operational conditions. However, ZIF-8 encapsulation faces several limitations: (1) restricted mass transport through its narrow pore apertures (~3.4 Å), which hinders the diffusion of bulky substrates; and (2) structural instability under acidic conditions or in the presence of chelating agents. Recent studies suggest that such protective encapsulation behavior may extend beyond ZIF-8 to other MOFs, such as MOF-545-Fe,[51] Tb-BTC,[52] Zn-MOF-74,[53] and UiO-66-F_4,[42] highlighting the broader role of MOFs in enhancing enzyme stability and facilitating substrate transport. For example, as illustrated in Fig. 3a, Zr^{4+} and tetrafluoroterephthalic acid can assemble into the ultrastable UiO-66-F_4 under mild conditions, which was employed to co-encapsulate alkaline phosphatase (ALP) and HRP. The MOF shell constructed around the enzymes effectively preserved their activity under harsh environments, such as elevated temperature and extreme pH, while the proximity of the two enzymes facilitated efficient cascade catalysis. As a result, the ALP-HRP@MOF nanocomposites exhibited markedly improved catalytic efficiency, enhanced selectivity, and robust operational stability.[42]

2.2.2.2. COFs. COFs exhibit superior chemical stability compared to MOFs due to their strong covalent linkages. However, conventional COF synthesis requires harsh conditions (elevated temperatures, organic solvents, and acid catalysts), which are not compatible for *in situ* enzyme encapsulation.[28] To reduce the risk of enzyme denaturation during COF crystallization, Chen reported a MOF-based sacrificial templating strategy to construct enzyme–COF biocatalysts.[54] This sacrificial templating concept can be extended to various COF hosts with similar properties. Although the mentioned template-protective assembly strategy could realize *de novo* encapsulation of enzymes into

COFs, its complexity limits the extension to various COFs hosts. Their group reported a biofriendly and scalable one-pot synthesis strategy for enzyme–COF biocatalysts using acetic acid under aqueous solution, and this method could be extended to various COFs.[55] However, due to the addition of enzyme-sensitive protonic acid, the practicality for different enzymes is still puzzled. Our group recently developed an aqueous-phase method that uses 2 μL of the 1-butyl-3-methylimidazolium dicyanamide ionic liquid catalyst to enable COF polymerization under enzyme-compatible conditions (Fig. 3b).[29] The obtained highly crystalline enzyme–COF biocatalysts brought about the rigorous sieving effect and enhanced capability for degradation of pollutants compared to their poorly crystalline counterpart. In addition to liquid-phase methods, mechanochemistry provides new insights for fabricating enzyme–COF biocatalysts. This approach minimizes the consumption of organic solvents and strong acid/base catalysts, circumventing the harsh conditions that are typically necessary for COF crystallization and avoiding enzymes denaturation. In addition, we also report a mechanochemistry-guided assembly strategy for the construction of enzyme@COFs.[56] The enzyme@COFs remain stable in a wider pH range (3–11), which expands the versatility and encourages further exploration in various environmental scenarios.

3. Environmental pollutant detection

The integration of enzymes with porous reticular frameworks has revolutionized the development of enzyme-based biosensors, greatly improving their performance in detecting environmental pollutants. These framework materials offer an ideal microenvironment for enzyme immobilization, which helps preserve catalytic activity and promotes efficient electron transfer and signal amplification. This section systematically examines the application of enzyme-immobilized porous reticular frameworks in the detection of diverse contaminants, including pesticides, phenolic compounds, antibiotics, microbial pathogens, and other emerging pollutants. Furthermore, the performance of representative hybrid biocatalysts is critically evaluated in terms of sensing efficacy (Table 1).

3.1. Pesticides

Pesticides have long been fundamental tools in global agriculture, playing a crucial role in safeguarding crop yield and quality by controlling pests, diseases, and weeds. However, the widespread and often excessive application of certain classes, such as organophosphorus pesticides (OPs) and carbamates, has led to their persistence in the environment and bioaccumulation across food chains, raising significant public health and ecological concerns.[57,58] In the era of smart agriculture, which emphasizes precision and sustainability, the development of real-time, on-site monitoring methods for pesticide residues has become increasingly vital.[3] To address this need, pesticide biosensors have evolved from conventional enzyme inhibition assays toward more sophisticated platforms, including those based on direct hydrolytic enzymes (*e.g.*, OPH, QpeH, and lipase) and immunoassay-based detection (ELISA).

AChE-based biosensors, whose detection mechanism for organophosphorus pesticides (OPs) is illustrated in Fig. 4a, represent one of the most extensively investigated platforms for pesticide detection.[59,60] To overcome limitations in enzyme stability and signal amplification, recent studies have integrated AChE with MOFs and COFs. This integration substantially improves both the operational lifetime and shelf stability of the biosensors, which are crucial for field-deployable analytical devices.[61–77] A representative example is the work by Cao *et al.*, who co-encapsulated AChE, HRP, and choline oxidase (CHO) within a cruciate flower-like ZIF-8 *via* a one-step co-precipitation method (Fig. 4b). Using acetylcholine (ATCh) as the substrate, the pesticide acephate inhibits AChE activity, thereby disrupting the enzymatic cascade and decreasing hydrogen peroxide (H_2O_2) production, leading to a measurable color change for colorimetric detection (Fig. 4c). The well-defined porous structure of CF-ZIF-8 provided a favorable micro-environment that maintained enzyme activity and spatial organization. This multi-enzyme platform showed a good linear relationship between the acephate concentration and the inhibition rate in the range of 0.001–1 μM and achieved a detection limit of 0.23 nM for acephate (Fig. 4d), demonstrating high sensitivity.[47]

Beyond serving as immobilization supports, recent studies demonstrate a paradigm shift toward frameworks that actively participate in signal transduction, either through intrinsic enzyme-mimetic activity (*e.g.*, Fe-based MOFs with peroxidase-like function) or by facilitating electron transfer in electrochemical systems. For example, Fe-based MOFs demonstrate peroxidase-like activity, enabling them to catalyze the oxidation of thiocholine (TCh), a hydrolysate of ATCh by AChE, into a chromogenic product. Inhibition of AChE by pesticides disrupts this catalytic process, producing a measurable signal change. Recent developments include multifunctional nanozymes such as C_{60}@MOF-545-Fe, in which host–guest interactions enhance both oxidase- and peroxidase-like activities, enabling cascade catalysis without external energy input.[51] The nanoconfined structure of this composite facilitates efficient molecular transport. When combined with AChE *via* supramolecular assembly, an enzyme–nanozyme continuous-flow reactor was constructed. This system not only allowed simultaneous detection of glyphosate, omethoate, and paraoxon but also discriminated among them *via* a three-channel sensor array (Fig. 4e). Furthermore, by integrating a YOLO v5-OPs deep learning model into a portable platform, direct terminal-based fitting equations were achieved, supporting rapid on-site analysis of organophosphorus pesticides (Fig. 4f). In parallel, confined catalytic systems such as V-TCPP(Fe)/AChE@ZIF have been designed for dual-mode colorimetric and chemiluminescence detection of pesticides like chlorpyrifos, achieving linear detection ranges of 1–50 nM (LOD 0.61 nM) and 1–40 nM (LOD 0.13 nM), respectively.[64] Another colorimetric strategy leverages the reaction between TCh and 5,5′-dithiobis (2-nitrobenzoic acid) (DTNB), generating yellow 2-nitro-5-thiobenzoic acid

Table 1 Summary of the reported enzyme-immobilized porous reticular frameworks used for environmental monitoring

Pollutants	Targets	Porous reticular frameworks	Enzymes	Detection methods	Ranges	LOD	Ref.
Pesticides	Acephate	ZIF-8	AChE/CHO/HRP	Colorimetric	0.001–1 μM	2.3×10^{-4} μM	47
	Chlorpyrifos	ZIF-8	AChE	Colorimetric	1–50 nM	0.61 nM	64
				Chemiluminescent	1–40 nM	0.13 nM	
	Chlorpyrifos	Zn-MOF-74	AChE	Colorimetric	1.0–600 ng mL^{-1}	1.0 ng mL^{-1}	53
	Carbaryl	COFThi-TFPB	AChE	Electrochemical	2.2–60 μM	0.22 μM	66
	Carbaryl	COFDhnda-BTH	AChE	Electrochemical	0.48–35.0 μM	0.16 μM	67
	DDVP	Ce/Zr-MOF	AChE/CHO	Colorimetric	0.5–500 ng mL^{-1}	0.32 ng mL^{-1}	61
	Ethyl paraoxon	ZIF-8	AChE/HRP	Colorimetric	6–800 ng mL^{-1}	1.8 ng mL^{-1}	49
	Glyphosate	NH_2-IMOF	AChE	Electrochemical	1×10^{-15}–1×10^{-9} M	1.24×10^{-13} M	68
	Isocarbophos	ZIF-8	AChE	Electrochemical	0.5–100 ng mL^{-1}	0.18 ng mL^{-1}	65
	Malathion	COF-DhaTab	AChE	Electrochemical	1–10 000 nM	0.5 nM	62
	Malathion	COFTFPB-DBD	AChE	Electrochemical	1×10^{-12}–1×10^{-8} g L^{-1}	3.0×10^{-13} g L^{-1}	63
	MP	ZIF-8	AChE/CHO	Fluorescence	1–5000 μg L^{-1}	0.23 μg L^{-1}	48
	MP	La-MOF-NH_2	AChE	Electrochemical	1.0×10^{-13}–5.0×10^{-9} g mL^{-1}	5.8×10^{-14} g mL^{-1}	69
	MP	MPNFs	AChE/CHO/HRP	Colorimetric	0.1–1000 nM	0.032 nM	70
	MP	MPNCs	AChE/CHO	Fluorescence	0.05–1000 nM	0.015 nM	71
	MP	*p*-COFs	AChE	Electrochemical	1.9×10^{-9}–3.8×10^{-5} M	2.3×10^{-10} M	72
	MP	Tb-BTC	OPH	Fluorescence	0.1–103 μM	2.6 nM	50
	MP	UiO-66-NH_2	OPH	Fluorescence	10–10^6 ng mL^{-1}	10 ng mL^{-1}	80
	MP	Cu-MOF	Lipase	Electrochemical	0.1–38 μM	0.067 μM	81
	MP	ZIF-8	Lipase BCL	Electrochemical	0.1–38 mM	0.28 mM	82
	MP	UiO-66	Lipase BCL	Electrochemical	5–40 μM	0.84 μM.	85
	Trichlorfon	COF-LZU1	AChE	Electrochemical	0.2–19 ng mL^{-1}	0.067 ng mL^{-1}	73
	Paraoxon	Aza-COFs	AChE	Electrochemical	10–1000 ng mL^{-1}	1.4 ng mL^{-1}	74
	Paraoxon	$Cu_3(THQ)_2$	AChE	Electrochemical	1–1000 ng mL^{-1}	0.37 ng mL^{-1}	75
	Malathion	ZIF-8	AChE	Electrochemical	3 pM-300 nM	1.10 pM	76
	Omethoate				4.69 pM-4.69 μM	1.32 pM	
	Glyphosate	MOF-545-Fe	AChE	Electrochemical	2.0–800 ng mL^{-1}	0.65 ng mL^{-1}	51
	Omethoate				0.5–800 ng mL^{-1}	0.16 ng mL^{-1}	
	Paraoxon				1.0–800 ng mL^{-1}	0.32 ng mL^{-1}	
	MP	COF-Bta-NSs	AChE	Electrochemical	5.0×10^{-13}–1.0×10^{-8} g mL^{-1}	2.04×10^{-13} g mL^{-1}	77
	Paraoxon				1.0×10^{-12}–1.0×10^{-8} g mL^{-1}	7.94×10^{-13} g mL^{-1}	
	Malathion				5.0×10^{-11}–1.0×10^{-7} g mL^{-1}	5.37×10^{-12} g mL^{-1}	
	Glyphosate	UiO-66-F_4	ALP/HRP	Colorimetric	0.02–6.67 μM	10.0 nM	42
	QpE	mZIF	QpeH/AOx	Colorimetric	8.2–214.6 $\times$ 10^{-6} M	2×10^{-6} M	50
	Nitrofen	UiO-66	CRL	Electrochemical	0–100 μM	0.016 μM	85
	Nitrofen	ZIF-8	BCL	Electrochemical	0–114 μM	0.46 μM	86
	Nitrofen	Cu-BTC	CRL	Electrochemical	0–78 μM	1.15 μM	87
	Nitrofen	COF-300	CRL	Chemiluminescence	0.02–50.0 μM	11 nM	90
	Chlorpyrifos	HP-UiO-66-OH	Cyt *c*	Colorimetric	10–10 000 pg mL^{-1}	4.63 pg mL^{-1}	93
	Imidacloprid	NSMOFs	HRP	Colorimetric	0.02–1.1 ng mL^{-1}	8.0 pg mL^{-1}	91
	Imidacloprid	MOFs-P	HRP	Smartphone	0.001- 500 ng mL^{-1}	0.0013 ng mL^{-1}	92
	Isocarbophos	COFs-PB	HRP	Colorimetric	0.05–1000 ng mL^{-1}	0.03 ng mL^{-1}	90
Phenolic contaminants	Phenol	BHb	ZIF-8	Colorimetric	0–200 μM	1 μM	94
	Phenol	HRP/GOx	ZIF-8	Colorimetric	20–300 μM	0.60 μM	45
	Phenol	HRP/GOx	H-ZIF-8-	Colorimetric	0–100 μM	0.86 μM	96
	Phenol	NiZn-MOF	Tyr	Electrochemical	0.08–58.2 mM	6.5 nM	98
	BPA	Cu-TCPP	Tyr	Electrochemical	3.5 nM-8.9 μM	1.2 nM	97
	BPA	ZIF-8	LAC	Electrochemical	0.01–0.4 mM	1.95×10^{-3} mM	44
	BHA	ZIF-8	HRP	Electrochemical	0.1–1600 μM	0.03 μM	95
	Catechol	ZIF-90	LAC	Electrochemical	20–400 μM	1.86 μM	99
Antibiotics	Tetracycline	UiO-66-NH_2	LAC	Electrochemical	1.0×10^{-6}–6.0×10^{-5} M	8.94×10^{-7} M	100
	Chloramphenicol	HRP	MAF-7	Colorimetric	0.005–6 ng mL^{-1}	0.51 pg mL^{-1}	101
	Streptomycin	HRP	Ce/Zr-UiO66	Colorimetric	0.01–5000 ng mL^{-1}	0.051 ng mL^{-1}	102
Microbial pathogens and mycotoxins	*Escherichia coli*	Cyt *c*	ZIF-8	Colorimetric	1–10^6 CFU mL^{-1}	1 CFU m^{-1}	46
	Escherichia coli	GOx	mZIF-8	Colorimetric	10–10^8 CFU mL^{-1}	10 CFU mL^{-1}	103
	S. aureus				30–10^8 CFU mL^{-1}	30 CFU mL^{-1}	
	S. aureus	ZIF-90	Urease	Colorimetric	10–10^9 CFU mL^{-1}	1.96 CFU mL^{-1}	104
	AFB1	PCN-224	HRP	Fluorescence and Colorimetric	100 pg mL^{-1}–10 ng mL^{-1}	0.65 pg mL^{-1}	109
	AFB1	HKUST-1	GOx	Colorimetric	0.01–0.1 ng mL^{-1}	0.004 ng mL^{-1}	105

Table 1 (*continued*)

Pollutants	Targets	Porous reticular frameworks	Enzymes	Detection methods	Ranges	LOD	Ref.
	Deoxynivalenol	GOx	PCN-224	Fluorescence and Colorimetric	0.01–1000 ng mL^{-1} 0–1000 ng mL^{-1}	0.0053 ng mL^{-1} 0.034 ng mL^{-1}	108
Other contaminants	As(v) H_2S	ACP/hemin PSSA-HRP	Zn-MOF ZIF-8	Fluorescence Chemiluminescence	3.33–300 μg L^{-1} 4.88–78.13 nM	1.05 μg L^{-1} 0.09 nM	110 112

(TNB) with a characteristic absorption at 412 nm. Based on this mechanism, AChE immobilized in Zn-MOF-74 was used to construct a biosensor that can detect chlorpyrifos with a limit of 1.0 ng mL^{-1}, demonstrating high potential for trace-level quantification.[53]

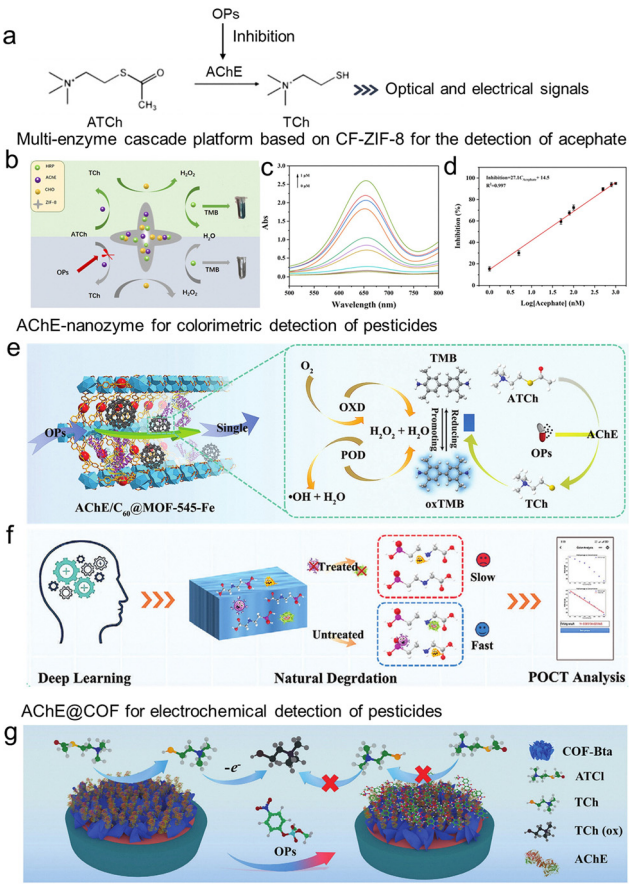

Fig. 4 AChE inhibition-based sensors for pesticide detection through the immobilization of enzymes on porous reticular frameworks. (a) The mechanism of ACh enzyme inhibition reaction sensors for the detection of OPs. (b) Schematic diagram of a high-performance multi-enzyme cascade platform for detecting organophosphorus. (c) The ultraviolet spectra of organophosphorus at different concentrations detected by enzyme cascade platform. (d) The linear curve of inhibition rate and logarithm of acephate concentration, reproduced from ref. 47 with permission from Elsevier, *Food Chem.*, 2022, **381**, 132282, copyright 2022. (e) Principle of AChE/C_{60}@MOF-545-Fe cascade flow reactor and (f) the application of a deep learning strategy, reproduced from ref. 51 with permission from Wiley, *Adv. Funct. Mater.*, 2024, **35**, 2419499, copyright 2024. (g) Detection mechanism of the electrochemical biosensing for OPs, reproduced from ref. 77 with permission from Wiley, *Adv. Funct. Mater.*, 2023, **33**, 2302917, copyright 2023.

In electrochemical biosensors, conductive MOFs or COFs serve as efficient electron-transfer mediators.[74,75,77,78] When AChE is immobilized on such materials, the electroactive product thiocholine is directly oxidized on the conductive framework, promoting efficient electron transfer to the electrode surface. This "electron-wiring" effect enhances amperometric signal strength and overall detection sensitivity. For instance, ultrathin COF nanosheets (COF-Bta-NSs) with a thickness of approximately 1.95 nm and enriched nitrogen/sulfur-containing bithiazole units have been developed (Fig. 4g).[77] The ordered porous structure with abundant unsaturated edge sites enables robust immobilization of AChE *via* supramolecular interactions and promotes local enrichment of analyte molecules. Moreover, the incorporation of N, S-rich bithiazole moieties enhances electrical conductivity, thereby improving biosensor detectability. Under optimized conditions, this biosensor exhibited exceptional performance in detecting OPs, featuring a broad detection range and ultralow detection limits (*e.g.*, methyl parathion (MP): 2.04 × 10^{-13} g mL^{-1}; paraoxon: 7.94 × 10^{-13} g mL^{-1}; and malathion: 5.37 × 10^{-12} g mL^{-1}), along with high selectivity and stability.

While AChE inhibition offers broad-spectrum detection, it inherently lacks selectivity among different pesticides. In contrast, direct hydrolytic enzymes provide superior specificity by recognizing distinct pesticide structures and catalyzing their hydrolysis. These enzymes enable the design of biosensing platforms that convert hydrolysis products into measurable signals, offering promising routes for selective and sensitive detection. Aryloxyphenoxypropionate (AOPP) herbicides are widely used for controlling grass weeds in broadleaf crops. Leveraging this specificity, Ma *et al.* developed a colorimetric biosensor by co-encapsulating a three-enzyme cascade that contains QpeH, alcohol oxidase (AOx), and peroxidase-mimicking magnetic ZIF-8 (mZIF-8) into a single framework.[50] As outlined in Fig. 5a, the sensing mechanism involves the QpeH-catalyzed hydrolysis of the AOPP herbicide, followed by AOx oxidation of the released alcohol, with mZIF-8 finally catalyzing the formation of a colored product for detection. This biosensor demonstrated high sensitivity for quizalofop-*P*-ethyl (QpE), achieving a linear detection range of 8.2 to 214.6 μM and a detection limit of 2 μM.

MP, a highly toxic organophosphorus pesticide, poses significant risks to human health and the environment due to its neurotoxic effects and environmental persistence.[79] Its

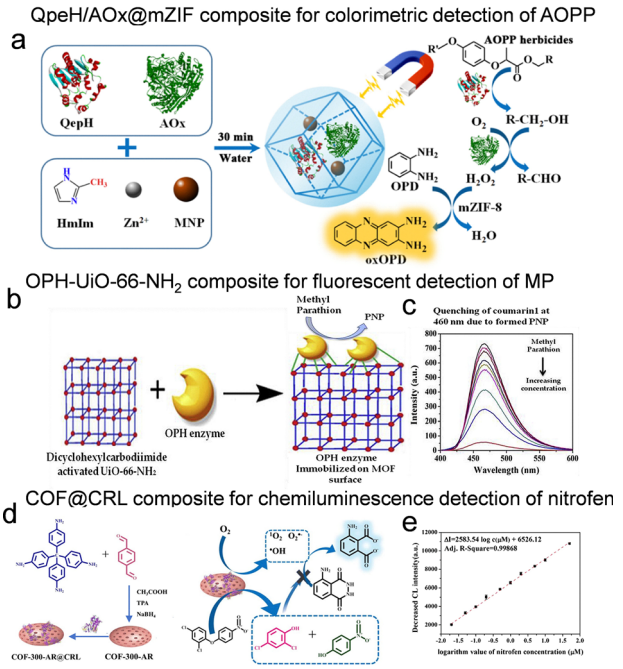

Fig. 5 Direct catalytic enzyme-based sensors for pesticide detection through the immobilization of enzymes on porous reticular frameworks. (a) Schematic illustration of the one-pot synthesis of QpeH/AOx@mZIF composite with magnetic collection and its use as a biosensor for the rapid detection of AOPP herbicides, reproduced from ref. 50 with permission from American Chemical Society, *ACS Appl. Mater. Interfaces*, 2021, **13**, 44329–44338, Copyright 2021. (b) Reaction mechanism of OPH^{6His}/UiO-66-NH_2 for fluorescence detection of MP. (c) The fluorescence intensity of MP at different concentrations, reproduced from ref. 80 with permission from Elsevier, *Environ. Res.*, 2019, **174**, 46–53, Copyright 2019. (d) Schematic diagram of COF-300-AR@CRL synthesis and chemiluminescence detection of nitrofen. (e) Linear calibration plot between the decreased chemiluminescence intensities and the logarithm values of nitrofen concentration in the 0.02–50.0 μM range, reproduced from ref. 88 with permission from Springer Nature. *Microchim. Acta*, 2023, **190**, 492, Copyright 2023.

detection has been effectively achieved using both OPH-based fluorescence sensing and lipase-based electrochemical approaches.[52,80–83] For fluorescence-based detection, the immobilization of hexahistidine-tagged OPH (OPH^{6His}) onto a zirconium-based MOF (UiO-66-NH_2) has been demonstrated. In this system, the immobilized enzyme catalyzes the hydrolysis of MP to *p*-nitrophenol (PNP), with the PNP concentration being directly proportional to the original pesticide concentration (Fig. 5b). The fluorescent reporter coumarin 1 is subsequently introduced, whose emission is quantitatively quenched by PNP (Fig. 5c). This OPH^{6His}/UiO-66-NH_2 composite not only enhanced enzymatic activity by approximately 37% but also maintained stability over 60 days and allowed at least eight reuse cycles. The sensing platform achieved a wide detection range of 10–10^6 ng mL^{-1} with a quantification limit of 10 ng mL^{-1} and was successfully validated in spiked food samples.[80] Electrochemical detection of MP has been realized using lipase immobilized on ZIF-8 and its amine-functionalized derivative. Lipase catalyzes the hydrolysis of MP to PNP, which is then electrochemically oxidized at the electrode interface. The lipase@ZIF-8/chitosan-modified glassy carbon electrode exhibited a low detection limit of 0.28 μM, a wide linear detection range, and good repeatability. The biosensor retained over 80% of its initial response after 20 days of storage, demonstrating excellent operational and storage stability. This system illustrates the effectiveness of MOF-immobilized lipase in facilitating both hydrolysis and subsequent electrochemical signal generation.[82]

As a representative diphenyl ether herbicide, nitrofen is widely used for weed control but poses considerable environmental and health hazards.[84] Recent studies have reported the development of electrochemical enzyme sensors incorporating lipases embedded in materials such as UiO-66, ZIF-8 or Cu-BTC.[85–88] These lipases catalyze the cleavage of the C–O–C bond in nitrofen, producing redox-active phenolic compounds. For example, Candida rugosa lipase (CRL) was immobilized on an amine-rich covalent organic framework (COF-300-AR) (Fig. 5d). The resulting COF-300-AR@CRL composite exhibited dual catalytic functions: the COF framework served as an oxidase mimic to catalyze the luminol-dissolved oxygen chemiluminescence reaction, while the immobilized CRL hydrolyzed nitrofen to release reducing phenolic compounds. These phenolic products effectively quenched the chemiluminescence signal, enabling the quantification of nitrofen in the range of 0.02–50.0 μM with a detection limit of 11 nM (Fig. 5e). This method displayed excellent precision (2.0% RSD for 50.0 nM nitrofen) and recyclability, and was successfully applied to vegetable and fruit samples.[88]

Despite the superior specificity of direct hydrolytic enzymes arising from their recognition of distinct pesticide structures, their practical application is hindered by a narrow spectrum of hydrolyzable substrates. ELISA presents a complementary and versatile alternative, offering robust analytical performance through the high specificity inherent in immunoreactions.[89] This platform not only enables sensitive detection of environmental contaminants but also exhibits remarkable adaptability, as its target recognition can be readily tailored to diverse pesticides by simply exchanging the antibody employed. Yan *et al.* developed an enzyme-engineered assembly strategy for *in situ* enzyme encapsulation within COFs-PB *via* a covalent–polymerization–permeation mechanism.[90] Capitalizing on this design, they fabricated an HRP@COFs-PB-based immunosensor for isocarbophos detection. In this competitive format, the coating antigen immobilizes on the plate, competing with the pesticide for primary antibody binding. The HRP-COFs-Ab2 conjugate recognizes the captured antibody and catalyzes the tetramethylbenzidine (TMB)/H_2O_2 chromogenic reaction, with signal intensity being inversely proportional to pesticide concentration (Fig. 6a). An obvious color attenuation of HRP-COFs composite-based ELISA is observed with an increase of isocarbophos concentration (Fig. 6b). Through G × B color processing, the authors achieved quantitative detection across 0.05–1000 ng mL^{-1} with a calculated LOD of 0.03 ng mL^{-1}, outperforming other color-algorithm methods and highlighting its potential for on-site pesticide monitoring (Fig. 6c and d). Similarly, HRP immobilized in other MOFs has shown specific

recognition capability in immunosensors for detecting imidacloprid.[91,92] Notably, such immunosensors typically require secondary antibodies. However, Chen *et al.* developed an innovative immunoassay platform for colorimetric detection of chlorpyrifos (CPF) that circumvents this requirement.[93] By modifying the ligand functional groups of MOFs, they precisely tuned the pore electronic properties and hydrophilic microenvironment, which enhanced both catalytic activity and stability of the immobilized enzyme system. The resulting HP-UiO-66-OH material not only serves as an enzyme immobilization platform but also functions as a recognition element for CPF through strong Zr–O–P interactions, thereby eliminating the need for secondary antibodies (Fig. 6e). As shown in Fig. 6f and g, the absorbance increased progressively with CPF concentration, exhibiting excellent linear correlation across the concentration range of 10–10 000 pg mL^{-1} when plotted against the logarithm of CPF concentration.

A critical challenge in this field is the persistent disconnect between laboratory performance and real-world applicability. Despite exceptional detection limits reported under optimized conditions, most systems remain unvalidated in complex environmental matrices or under variable field conditions. Furthermore, the scalability and cost-effectiveness of these platforms have yet to be systematically explored.

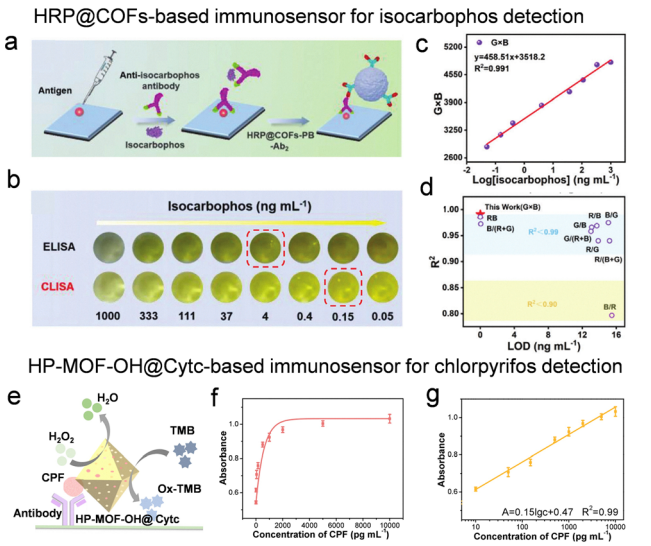

Fig. 6 The immunosensor for pesticide detection through the immobilization of enzymes on porous reticular frameworks. (a) Schematic illustration of HRP@COFs-PB-based competitive immunosensor for imidacloprid detection. (b) The color change of HRP-COFs composite-based CLISA with the increase of isocarbophos concentration. (c) The relationship between the G × B value response and isocarbophos concentration. (d) Comparison of detection limits between the G × B algorithm and other algorithms, reproduced from ref. 90 with permission from Wiley, *Adv. Funct. Mater.*, 2025, **35**, 2420159, copyright 2025. (e) Schematic illustration of the HP-UiO-66-OH@Cytc-based immunoassay platform for CPF detection. (f) Calibration curve and (g) linear detection range of HP-UiO-66-OH@Cytc-based ELISA, reproduced from ref. 93 with permission from American Chemical Society, *Anal. Chem.*, 2025, **97**, 16019–16025, copyright 2025.

3.2. Phenolic contaminants

Phenolic contaminants, extensively generated by industrial sectors such as textiles, plastics, and paper manufacturing, represent a major class of persistent environmental pollutants.[4] Their significant ecological and human health risks, which arise from resistance to degradation, bioaccumulative potential, and multifaceted toxicity, underline the critical need for reliable analytical methods for their detection. Among various strategies, oxidoreductase-based biosensors have gained considerable attention as a sustainable and effective detection platform. For instance, a bovine hemeprotein–zeolitic imidazolate framework-8 hybrid was designed to exhibit enhanced peroxidase-like catalytic activity, improved operational stability, and facilitated enzyme reuse. Leveraging these properties, in the presence of phenol and 4-aminoantipyrine, a colorimetric biosensing platform was constructed for the fast and sensitive detection of phenol, achieving a detection limit of 1.0 μM and a wide linear detection range of 0–200 μM through naked-eye visualization.[94] To further enhance performance, Au nanoparticles were introduced into hollow ZIF-8 improving its electrochemical behavior (Fig. 7a). The cavity of hollow ZIF-8 enhances the diffusion of substrates like butylated hydroxyanisole (BHA), while its superhydrophilic surface facilitates greater adsorption of reactant molecules, thereby accelerating electrochemical reactions. The electrochemical sensor demonstrates remarkable electrocatalytic activity toward BHA detection, with a broad linear response range from 0.1 to 1600 μmol L^{-1} and a detection limit as low as 0.03 μmol L^{-1}.[95]

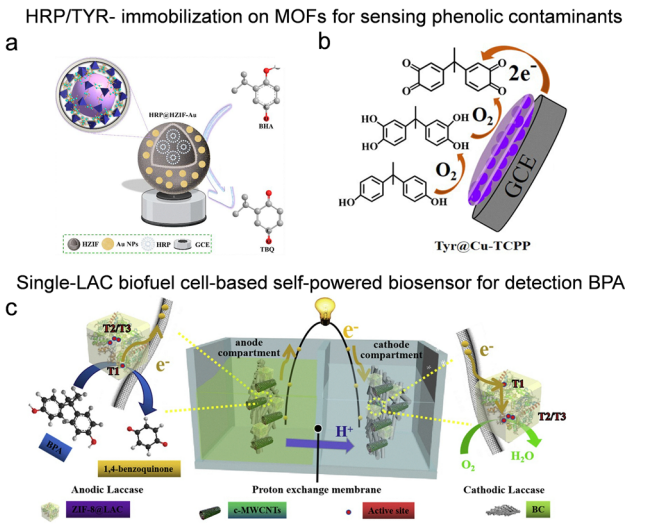

Fig. 7 Enzyme-immobilized porous reticular framework-based sensors for phenolic contaminants detection. (a) Electrochemical oxidation mechanism of BHA, reproduced from ref. 94 with permission from American Chemical Society, *ACS Appl. Mater. Interfaces*, 2016, **8**, 29052–29061. Copyright 2023. (b) Schematic mechanism of BPA biosensor with enhanced stability based on tyrosinase assembled between 2D Cu-TCPP nanofilms, reproduced from ref. 97 with permission from Elsevier, *Chem. Eng. J.*, 2022, **446**, 137001, copyright 2022. (c) Schematic illustration of a single-LAC biofuel cell with BPA as the fuel and O_2 as the final electron acceptor, reproduced from ref. 44 with permission from Elsevier, *Nano Energy*, 2020, **68**, 104308, copyright 2019.

A significant challenge in peroxidase-based sensing is the reliance on H_2O_2, an essential but costly and unstable co-substrate. To circumvent the need for exogenous H_2O_2, innovative multi-enzyme systems have been developed. In a representative work,[96] GOx and HRP were co-encapsulated within H-ZIF-8 to establish a cascaded biocatalytic system. This setup enables *in situ* H_2O_2 generation through GOx-catalyzed glucose oxidation, which subsequently activates spatially adjacent HRP for phenol detection. This system achieved a rapid colorimetric response with a linear detection range of 0–100 μM and a low LOD of 0.86 μM. Beyond HRP, the immobilization of laccase or tyrosinase (TYR) in porous crystalline frameworks has emerged as a powerful strategy for electrochemical sensing. Ma *et al.* developed an ultrasensitive electrochemical biosensor by assembling tyrosinase within two-dimensional Cu-TCPP nanosheets.[97] As bisphenol A (BPA) is a natural substrate for tyrosinase, the enzyme specifically catalyzes its oxidation, generating a ''signal-on'' response (Fig. 7b), which allowed for BPA monitoring with an impressive LOD of 1.2 nM. Similarly, TYR immobilized on 2D bimetallic NiZn-MOF and laccase encapsulated in ZIF-90 (LAC@ZIF-90) have also demonstrated outstanding performance in the electrochemical detection of phenol and catechol, respectively.[98,99]

Conventional electrochemical sensing requires an external power source. To minimize energy consumption, a breaking approach integrates biosensing with energy harvesting, creating self-powered sensors. Li *et al.*[44] developed highly flexible electrodes by encapsulating LAC in ZIF-8 and integrating them with a bacterial cellulose/carboxylated multi-walled carbon nanotube (BC/c-MWCNT) backbone (Fig. 7c). This BC/c-MWCNT/ZIF-8@LAC electrode was utilized as both the cathode and the anode in a single-enzyme enzymatic biofuel cell to construct a self-powered sensing platform for BPA. The oxidation of BPA by LAC generates an electric current, and the maximum power density of the EBFC was positively and linearly correlated with BPA concentration, achieving an LOD of 1.95 nM.

Despite notable innovations, most reported systems focus on model phenolic compounds (phenol, BHA, and BPA) with limited validation against complex mixtures of structurally similar contaminants commonly encountered in environmental samples. The selectivity of these platforms in real-world matrices remains inadequately characterized.

3.3. Antibiotics

The escalating overuse of antibiotics has resulted in the persistent presence of pharmaceutical contaminants in the environment and accelerated the spread of antimicrobial resistance (AMR). Residual antibiotics not only threaten the ecosystem but can also enter the human body through the food chain, further exacerbating AMR.[5] Consequently, the development of accurate and reliable analytical methods for monitoring antibiotics is essential to mitigate these risks.

LAC-based biosensors represent a promising approach for direct antibiotic detection. For instance, Zhong *et al.*[100] successfully constructed a LAC-modified electrochemical biosensor for tetracycline (TC) detection in food samples. By immobilizing LAC within a mesoporous carbon sphere (MCS)@UiO-66-NH_2 core–shell composite, they developed a sensing platform with enhanced enzymatic stability and electrocatalytic activity (Fig. 8a). The biosensor demonstrated satisfactory analytical performance, with a detection limit of 8.94×10^{-7} mol L^{-1}, a linear detection range of 1.0×10^{-6} to 6.0×10^{-5} mol L^{-1}, and good operational stability, making it suitable for screening antibiotic residues in complex food matrices.

LAC-based biosensors offer simplicity but are inherently limited to antibiotics that serve as enzyme substrates, restricting their applicability to a narrow subset of antibiotic classes. In contrast, aptamer- or antibody-based platforms provide broader applicability, as the recognition element can be tailored to any antibiotic by simply replacing the aptamer sequence. These systems typically utilize encapsulated enzymes for signal transduction and amplification, enabling highly sensitive detection across various sample types. A representative example is a portable colorimetric platform that integrates an aptamer-modified MOF for on-site antibiotic screening.[101] Specifically, HRP was encapsulated *in situ* within the hydrophilic MAF-7, effectively suppressing enzyme aggregation and enhancing catalytic activity. Aptamers were modified on the material surface *via* π–π stacking, forming an intelligent Aptamer (Apt)/HRP@MAF-7 probe for targeted antibiotic recognition. During detection, the binding between the aptamer and the target triggers the release of HRP activity, catalyzing the oxidation of TMB (Fig. 8b). The resulting color signal was accurately quantified using a handheld colorimeter. Using streptomycin as a model analyte, the sensor exhibited a wide linear detection range from 0.005 to 6 ng mL^{-1} and a detection limit of 0.51 pg mL^{-1}. This design can be adapted to different antibiotics by replacing the corresponding aptamer, making it highly valuable for field-deployable environmental and food safety monitoring.

To improve selectivity and reduce interference from complex sample matrices, pre-enrichment and separation of target analytes are effective strategies. Innovative platforms combining magnetic solid-phase extraction with enzymatic signal amplification have been developed. The researchers employed bimetallic MOF-based probes with dual functionality: efficient magnetic enrichment of target antibiotics and catalytic signal enhancement (Fig. 8c). In this system, Fe_3O_4@SiO_2 serves as a magnetic core supporting Ce/Zr-UiO-66 with a high specific surface area, enabling efficient enrichment and rapid separation of chloramphenicol. Furthermore, the synergistic catalysis between HRP and Ce/Zr-UiO-66 allowed broad linear detection from 0.1 to 100 ng mL^{-1} on an immunosensing platform, achieving a sensitivity of 51.3 pg mL^{-1}.[102] It should be noted that this versatility comes at the cost of increased complexity and additional functionalization steps, a trade-off that must be considered for different application scenarios.

3.4. Microbial pathogens and mycotoxins

The contamination of water and food by microbial pathogens presents a substantial threat to global public health. According to the World Health Organization, waterborne diseases, such as

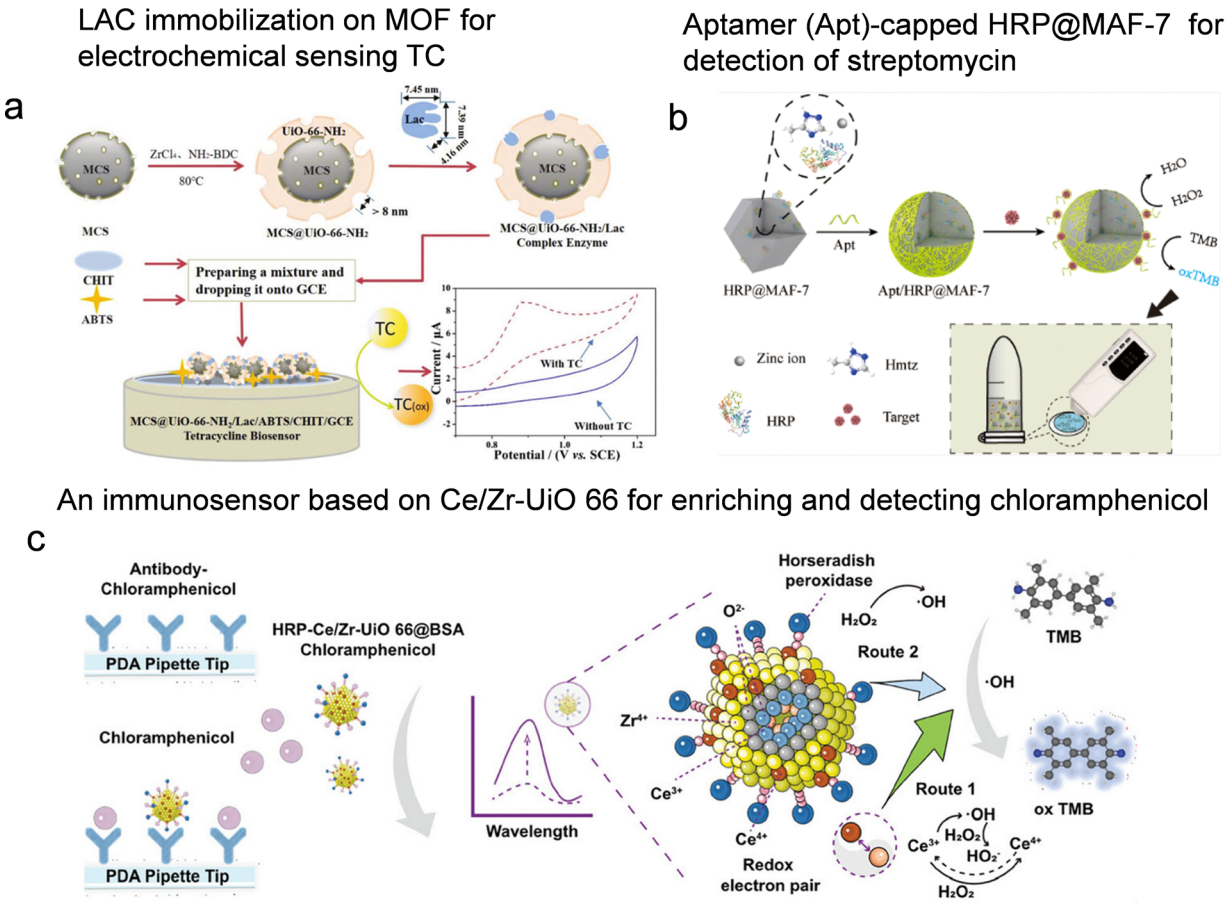

Fig. 8 Enzyme immobilization on porous reticular framework-based sensors for antibiotics detection. (a) Illustration of the synthesis process of the MCS@UiO-66-NH_2/LAC complex enzyme and construction of the MCS@UiO-66-NH_2/LAC/ABTS/CHIT/GCE tetracycline biosensor, reproduced from ref. 100 with permission from Royal Society of Chemistry, *Analyst*, 2021, **146**, 2825–2833, copyright 2021. (b) The principle of the Apt/HRP@MAF-7 sensor for on-site sensitive detection of targets, reproduced from ref. 101 with permission from American Chemical Society, *Anal. Chem.*, 2020, **92**, 14259–14266, copyright 2020, (c) schematic diagram of sensitive detection of chloramphenicol based on a dual-track multifunctional MOF-based biosensor with HRP-Ce/Zr-UiO-66@BSA-CAP and double catalysis of Ce^{3+}/Ce^{4+} and HRP, reproduced from ref. 102 with permission from Wiley, *Small*, 2024, **20**, e2309075, copyright 2024.

cholera, dysentery, typhoid, and polio, account for approximately 3.4 million deaths annually.[6] The rapid proliferation of pathogenic bacteria underscores the need for early and sensitive detection methods. Recently, biosensing platforms based on enzyme-immobilized porous reticular frameworks have emerged as promising tools for rapid, on-site pathogen monitoring.

Gao *et al.*[103] developed a portable pH-based biosensor utilizing GOx conjugated with mZIF-8. The mZIF-8/GOx conjugate was formed *via* electrostatic interactions. In this design, GOx activity remains suppressed until the target bacteria competitively bind to mZIF-8, triggering enzyme release and restoring catalytic function (Fig. 9a). The subsequent conversion of glucose to gluconic acid induces a measurable pH shift, enabling the detection of *Escherichia coli* and *Staphylococcus aureus* (*S. aureus*) with limits as low as 10 CFU mL^{-1} and 30 CFU mL^{-1}, respectively. This low-cost and user-friendly biosensor is well-suited for monitoring the quality of contaminated drinking water. Similarly, Li *et al.*[104] designed an enhanced immunoassay by encapsulating urease (U) within ZIF-90 through *in situ* synthesis (Fig. 9b). The resulting U@ZIF-90 composite was conjugated with antibodies for specific detection of *S. aureus*. The encapsulation not only increased enzyme loading and stability but also enhanced catalytic activity 3-fold due to the confinement effect. By quantifying urea hydrolysis, which induced pH changes detectable using a portable pH meter, the assay achieved a detection limit of 1.96 CFU mL^{-1} for *S. aureus* with high specificity. Its successful application in milk samples further demonstrated its potential for safeguarding infant food safety.

Beyond microbial pathogens, mycotoxins, which are secondary metabolites produced by certain fungi, also pose serious risks of contamination of water resources and agricultural products. These toxins can induce multiple adverse effects in humans, including causing damage to the neuroendocrine, gastrointestinal, reproductive, and immune systems.[106] Thus, establishing highly sensitive and accurate detection methods is essential.

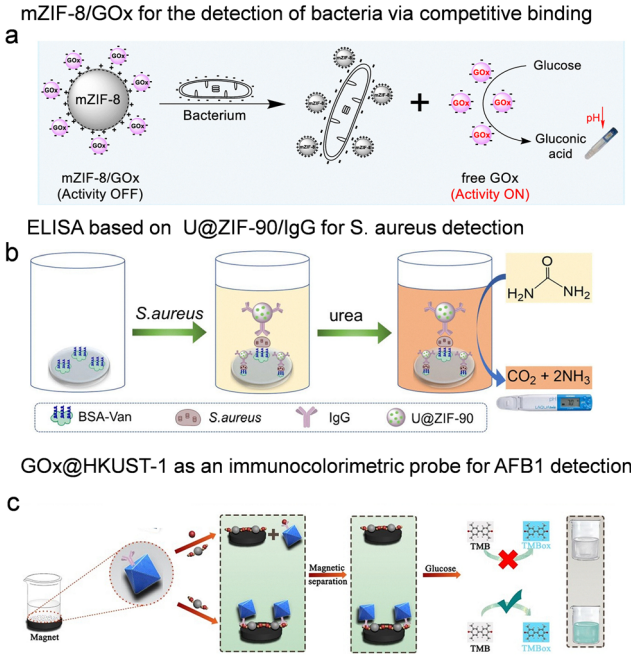

Fig. 9 Enzyme immobilization on porous reticular framework-based sensors for detection of microbial pathogens and mycotoxins. (a) Schematic illustration of the working principle of mZIF-8/GOx conjugate for the detection of bacteria by using a pH meter as a readout, reproduced from ref. 103 with permission from American Chemical Society, *ACS Appl. Mater. Interfaces*, 2023, **15**, 31224–31232, copyright 2023. (b) Illustration of the construction of ELISA based on U@ZIF-90/IgG for *S. aureus* detection with a pH meter as a readout, reproduced from ref. 104 with permission from Springer Nature, *Microchim. Acta*, 2022, **189**, 358, copyright 2022. (c) Schematic illustration of the synthesis of GOx@HKUST-1 @antibody and measuring principle of AFB1 sensor, reproduced from ref. 105 with permission from Elsevier, *Sens. Actuators B Chem.*, 2022, **369**, 132362, copyright 2022.

Aflatoxins (AFs), predominantly produced by *Aspergillus flavus* that contaminate crops and food stored under unsuitable conditions, rank among the most widely investigated mycotoxins.[107] To enable sensitive and stable AF detection, Zhang *et al.*[105] developed a multifunctional immunoprobe based on HKUST-1 (Fig. 9c). By employing an *in situ* encapsulation strategy, GOx and specific antibodies were incorporated into the framework. This composite material exhibits three key functions: enzyme immobilization, antibody support, and peroxidase-like activity. In the designed immunoassay, AFB1- and AFB1-coated magnetic beads compete for the binding sites on the immunoprobes. Unbound immunoprobes trigger a colorimetric cascade reaction: GOx catalyzes the oxidation of glucose to generate H_2O_2, which subsequently oxidizes TMB to form a blue-colored product. The intensity of this colorimetric signal is inversely proportional to AFB1 concentration. This method demonstrated a linear detection range of 0.01–0.1 ng mL^{-1} for AFB1, with a detection limit as low as 0.004 ng mL^{-1}. Notably, the detection limit was 126-fold lower than that achieved by conventional ELISA.

Recognizing that single-mode detection is susceptible to environmental interference, recent work has embraced dual-signal platforms. These self-validating systems enhance reliability by providing orthogonal confirmation, a crucial feature for regulatory applications where false positives or negatives carry significant consequences. Hong *et al.* constructed a cascade catalytic system using PCN-224 loaded with Pt nanoparticles and GOx for the detection of deoxynivalenol.[108] In this design, GOx catalyzes glucose to generate H_2O_2, which subsequently activates Pt nanoparticles to catalyze the TMB colorimetric reaction. Fluorescence signals are generated *via* Zr–O–P binding of fluorescent DNA. This dual-mode platform achieved limits of detection of 34 pg mL^{-1} (colorimetric) and 5.3 pg mL^{-1} (fluorescence), combining high sensitivity with reliability. Similarly, the same group also reported a dual-mode colorimetric and fluorescence method using PCN-224 loaded with HRP for sensing AFB1.[109] Despite impressive detection limits, the stability of antibody-functionalized probes in complex food matrices remains problematic. Non-specific binding and batch-to-batch variability in antibody performance represent the underaddressed obstacles to commercialization.

3.5. Other contaminants

In addition to organic pollutants, well-designed porous framework-based enzyme biosensing systems have been effectively extended to the detection of other chemical contaminants, such as heavy metal ions and toxic gases. For instance, Xu *et al.* constructed a ratiometric fluorescent platform for detecting arsenate (As(v)) using a Zn-MOF co-encapsulating acid phosphatase (ACP) and hemin.[110] This system operates on an enzyme-mediated signal switching mechanism: the inherent fluorescence of the MOF at 452 nm is quenched during the oxidation of *o*-phenylenediamine (OPD) to a fluorescent product (564 nm). The introduction of ascorbic acid 2-phosphate (AAP) suppresses this oxidation *via* enzymatic hydrolysis, restoring the original signal. As(v) inhibits ACP, preventing AAP hydrolysis and reactivating OPD oxidation, thereby enabling quantifiable As(v) detection with high selectivity, a linear detection range of 3.33–300 μg L^{-1}, and a detection limit of 1.05 μg L^{-1} (Fig. 10a and b).

Hydrogen sulfide (H_2S), a significant bioactive substance and a typical environmental pollutant, poses serious health and environmental risks. High concentrations of H_2S can cause respiratory irritation, and prolonged exposure may lead to unconsciousness or cardiac arrest; in addition, it contributes to air and water contamination as well as metal structure corrosion.[111] To address this, we developed a chemiluminescence sensor based on polystyrolsulfon acid (PSSA)-HRP@ZIF-8. This biocomposite activates luminol to produce chemiluminescence, which is selectively suppressed in the presence of H_2S due to inhibition of the biocatalyst (Fig. 10c). The resulting decrease in emission intensity allows for highly sensitive H_2S detection, with a linear detection range from 4.88 nM to 5 μM and a remarkable detection limit of 0.09 nM (Fig. 10d), demonstrating suitability for environmental and biological monitoring.[112]

While proof-of-concept studies have demonstrated remarkable analytical performance, systematic investigation of cross-reactivity

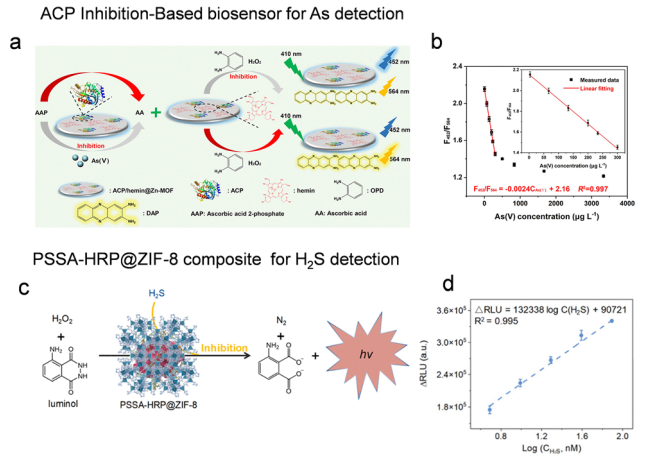

Fig. 10 Enzyme immobilization on porous reticular framework-based sensors for heavy metal ions and toxic gases. (a) Schematic illustration of the fluorescence detection of inorganic As(v) by using ACP/hemin@Zn-MOF composite. (b) The relationship between the fluorescence ratio F_{452}/F_{564} and the concentration of inorganic As(v), reproduced from ref. 110 with permission from Elsevier, *J. Hazard. Mater.*, 2021, **412**, 124407, copyright 2021. (c) Schematic illustration of H_2S sensing based on the PSSA-HRP@ZIF-8 composite combined with the luminol-H_2O_2 system. (d) The linear detection range for H_2S quantification, reproduced from ref. 112 with permission from the Royal Society of Chemistry, *Chem. Sci.*, 2024, **15**, 19609–19618, copyright 2024.

and interference from co-existing environmental constituents remains limited. This concern is particularly pronounced for enzyme inhibition-based sensors, where numerous environmental substances can interfere with color development, leading to potential false positives or inaccurate quantification. Consequently, selectivity claims require rigorous validation against panels of structurally similar compounds and common matrix components to establish reliable performance in complex environmental settings.

4. Conclusions and future perspectives

Environmental contaminants pose escalating threats to global ecosystem stability and public health, creating an urgent demand for advanced sensing platforms that enable accurate, on-site detection and quantification of pollutants. The integration of natural enzymes with porous reticular frameworks has established an innovative platform for developing robust hybrid biocatalysts. This nanobiotechnological approach synergistically combines exceptional catalytic functionality with structural programmability, providing a green route for constructing high-performance biocatalytic systems. These composites exhibit enhanced stability, superior catalytic performance, and remarkable detection sensitivity, offering promising avenues for real-time monitoring of diverse environmental contaminants. However, several scientific and technical challenges must be addressed before achieving widespread practical implementation (Fig. 11).

4.1. Substrate diffusion and mass transfer limitations

The confined pore architectures of porous reticular frameworks often hinder substrate accessibility to encapsulated enzymes, resulting in reduced catalytic efficiency compared to homogeneous reaction systems. Although reticular frameworks provide molecular-scale enzyme accessibility, mass transfer efficiency remains limited under diffusion-controlled conditions. Structural engineering strategies such as introducing hierarchical or defective pores *via* soft- or hard-templating methods can facilitate pollutant diffusion to enzymatic active sites without compromising framework stability.[39,113,114] Additionally, optimizing surface functionalization enhances interfacial compatibility and molecular transport.[93] The spatial preorganization of enzymes establishes a favorable channeling effect between proximal enzymes, significantly accelerating cascade reaction rates.[115] Combining pore architecture modulation with biomolecular spatial design offers a viable route to overcome diffusion limitations and enhance biosensor detection sensitivity.

4.2. Enhanced anti-interference capability for operation in complex matrices

The reliable deployment of sensors in real-world applications critically depends on their capacity to retain high performance when exposed to intricate sample environments. Sustaining catalytic activity and structural integrity under such conditions, particularly in the presence of salts, humic acids, and microorganisms, represents a formidable challenge. A major impediment is biofouling, *i.e.*, the undesirable accumulation of proteins, biomolecules, and microbes on sensor surfaces. This non-specific adsorption can obstruct active sites, diminish selectivity, and ultimately degrade sensor reliability and operational lifespan.[116] To mitigate these effects, systematic evaluation of anti-interference performance under laboratory-simulated real-matrix conditions is essential. Effective management of non-specific interactions necessitates deliberate interfacial engineering. Two principal strategies include: (1) implementing antifouling surface modifications: coating sensor interfaces with zwitterionic polymers or polyethylene glycol to form a bio-inert layer that minimizes non-specific adsorption of interfering species; and (2) engineering selective physical barriers:[117] precisely tailoring pore apertures or fabricating hierarchical structures to sterically exclude larger matrix components while preserving permeability for target analytes.

4.3. Expanding the detection spectrum

While enzyme-porous reticular framework hybrid sensors have shown effectiveness in detecting conventional targets, their broader application is limited by the inherent substrate specificity of the incorporated enzymes. To significantly expand the range of detectable analytes, particularly emerging contaminants such as perfluorinated compounds and microplastics, future work should focus on overcoming this enzymatic constraint. This can be accomplished through the discovery of novel enzyme activities or the rational engineering of existing enzymes to tailor their recognition and catalytic properties.

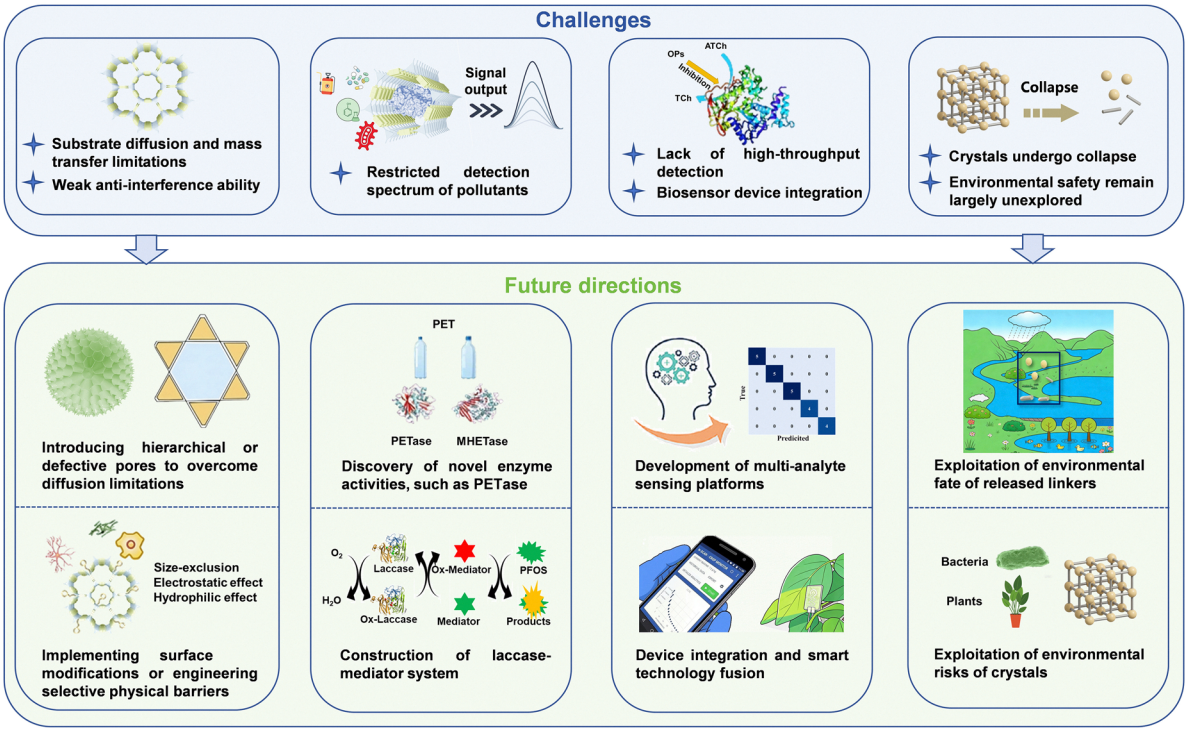

Fig. 11 The challenges and future directions of enzyme–porous reticular framework hybrids for environmental pollutant monitoring.

For example, nano-polyethylene terephthalate is hydrolyzed synergistically by cutinase and lipase to terephthalic acid, which is then sensitively detected using bromocresol purple as an indicator.[118] Additionally, LAC, especially when used with mediators, has demonstrated the ability to degrade perfluorinated compounds, suggesting its potential for sensing applications.[119]

4.4. Development of multi-analyte sensing platforms

Environmental contamination typically involves complex pollutant mixtures, presenting particular challenges for AChE inhibition-based sensors where specific pollutant identification remains difficult. Future development should focus on multiplexed sensor arrays capable of simultaneous detection of multiple contaminants.[49,120] These integrated platforms, comprising multiple responsive elements, offer advantages including rapid response, high scalability, and multi-functional compatibility. The incorporation of artificial intelligence (AI) technologies, particularly machine learning and deep learning algorithms, represents a crucial advancement. In systems employing colorimetric, electrochemical, or fluorescence-based detection, AI significantly enhances signal interpretation and noise reduction. More importantly, by leveraging pattern recognition and data fusion techniques, AI algorithms can deconvolute complex cross-reactive signals generated by sensor arrays, thereby enabling the precise identification and accurate quantification of each pollutant within high-throughput multiplexed assays. This capability is essential for resolving the composition of contaminant mixtures and avoiding false positives or negatives.[121,122] Furthermore, AI-enabled platforms can analyze complex datasets to predict contamination risks, assess spatiotemporal pollution trends, and support real-time decision-making.

4.5. Device integration and smart technology fusion

Translating laboratory biosensing platforms into robust, user-friendly, mass-producible devices presents a significant interdisciplinary challenge. The seamless integration of high-sensitivity biosensors into wearable systems or internet of things (IoT) networks enables continuous, real-time environmental monitoring. Recent advances in wearable sensor technology, initially developed for biomedical applications, offer promising avenues for environmental monitoring. The integration of flexible electronics with nanomaterials enables novel approaches for direct *in situ* detection of plant physiological signals.[123] Plant nanobionic technology has successfully transformed wild spinach into living sensors for detecting nitroaromatic compounds in groundwater by embedding single-walled carbon nanotubes within leaf tissues.[124] This innovative approach addresses quantitative calibration challenges and individual variability while demonstrating practical remote monitoring capabilities. The convergence of these platforms with smartphone interfaces, IoT networks, and AI algorithms enables real-time data transmission, automated analysis, and predictive modeling, transforming environmental monitoring into proactive, intelligent networks with significant implications for precision agriculture and environmental security.

4.6. Exploitation of environmental safety

Given that the proposed biocatalytic frameworks are intended for environmental pollutant monitoring, where they may be

directly deployed in natural water bodies or ecosystems, it is essential to evaluate not only their analytical performance but also their potential environmental risks. These porous crystals may undergo structural collapse after long-term use or upon exposure to complex environmental conditions, potentially releasing constituent metal ions and organic linkers into the surrounding water, which raises concern.[125] Such degradation products could themselves act as contaminants, leading to secondary pollution that undermines the purpose of monitoring. Another critical consideration is the emerging evidence that the frameworks can migrate through the aquatic food chain and bioaccumulate in organisms.[126] If scaffold fragments accumulate in biota, they may pose ecological hazards that outweigh the benefits of pollutant monitoring. At present, the environmental fate and long-term biosafety of these porous crystals remain largely unexplored. Therefore, future research efforts should prioritize investigating the ecotoxicity, degradation behavior, and bioaccumulation potential of these scaffolds to ensure the sustainable and safe application of this promising technology.

Author contributions

All authors have discussed the organization and presentation of the content and participated in the writing and editing of this Review Article.

Conflicts of interest

There are no conflicts to declare.

Abbreviations

MOFs	Metal–organic frameworks
COFs	Covalent organic frameworks
PEP	Pepsin
GOx	Glucose oxidase
MP-11	Microperoxidase-11
Tb-mesoMOF	Terbium-based mesoporous MOF
LAC	Laccase
HRP	Horseradish peroxidase
Cyt *c*	Cytochrome *c*
ALP	Alkaline phosphatase
AChE	Acetylcholinesterase
OPs	Organophosphorus pesticides
ATCh	Acetylcholine
CHO	Choline oxidase
H_2O_2	Hydrogen peroxide
TCh	Thiocholine
LOD	Limit of detection
DTNB	5,5′-dithiobis (2-nitrobenzoic acid)
TNB	2-nitro-5-thiobenzoic acid
MP	Methyl parathion
QpeH	Aryloxyphenoxypropionate herbicide hydrolase
OPH	Organophosphate hydrolase
AOPP	Aryloxyphenoxypropionate
AOx	Alcohol oxidase
QpE	Quizalofop-P-ethyl
PNP	*p*-Nitrophenol
mZIF-8	Magnetic ZIF-8
CRL	Candida rugosa lipase
BCL	*Burkholderia cepacia* lipase
ELISA	Enzyme-linked immunosorbent assays
TMB	Tetramethylbenzidine
CPF	Chlorpyrifos
BHA	Butylated hydroxyanisole
TYR	Tyrosinase
BPA	Bisphenol A
AMR	Antimicrobial resistance
TC	Tetracycline
MCS	Mesoporous carbon sphere
Apt	Aptamer
S. aureus	*Staphylococcus aureus*
U	Urease
AFs	Aflatoxins
As(v)	Arsenate
ACP	Acid phosphatase
OPD	*o*-phenylenediamine
AAP	Ascorbic acid 2-phosphate
H_2S	Hydrogen sulfide
PSSA	Polystyrolsulfon acid
AI	Artificial intelligence
IoT	Internet of Things

Data availability

All data discussed in this review originate from the studies cited throughout the manuscript. Readers seeking detailed experimental procedures, analytical methods or supplementary data sets can refer to the corresponding publications listed in the References section.

Acknowledgements

We acknowledge financial support from projects of the National Natural Science Foundation of China (22104159, 22174164, and 22506069), the Guangdong Basic and Applied Basic Research Foundation (2024B1515020070, 2023A15150 11632, and 2022A1515010837), the National High-Level Talents Special Support Program-Young Talents (2024WRQB006), the Fundamental Research Funds for the Central Universities, Sun Yat-sen University (23lgbj005), the Science and Technology Planning Project of Sichuan Province (No. 2025NSFSC2058), the Guangdong Basic Research Center of Excellence for Functional Molecular Engineering (31000-42080002), and the Natural Science Foundation of Guangzhou City (202201011408).

Notes and references

1 V. K. Gaur, P. Sharma, R. Sirohi, M. K. Awasthi, C.-G. Dussap and A. Pandey, *J. Hazard. Mater.*, 2020, **398**, 123019.

2 M. M. McAlister, Q. Zhang, J. Annis, R. W. Schweitzer, S. Guidotti and J. R. Mihelcic, *Environ. Sci. Technol.*, 2022, **56**, 732–738.
3 Y. Wang, H. Li and X. Yan, *TrAC, Trends Anal. Chem.*, 2025, **191**, 118381.
4 R. Sridar, U. U. Ramanane and M. Rajasimman, *Environ. Nanotechnol., Monit. Manage.*, 2018, **10**, 388–393.
5 M. A. Cook and G. D. Wright, *Sci. Transl. Med.*, 2022, **14**, eabo7793.
6 F. Y. Ramírez-Castillo, A. Loera-Muro, M. Jacques, P. Garneau, F. J. Avelar-González, J. Harel and A. L. Guerrero-Barrera, *Pathogens*, 2015, **4**, 307–334.
7 C. K. Ho, A. Robinson, D. R. Miller and M. J. Davis, *Sensors*, 2005, **5**, 4–37.
8 J. Devers, D. I. Pattison, A. B. Hansen and J. H. Christensen, *Talanta*, 2025, **282**, 127032.
9 R. Pei, L. Ye and C. Jing, *Biosens. Bioelectron.*, 2023, **229**, 115244.
10 S. Liu, C. Nie, F. He, G. Wu, H. Wang, S. Li, C. Du, Z. Zheng, J. Cheng, Y. Shen and J. Cheng, *Trends Food Sci. Technol.*, 2024, **150**, 104597.
11 M. Bilal, A. K. Singh, H. M. N. Iqbal and G. Boczkaj, *Chem. Eng. J.*, 2023, **474**, 145020.
12 Z. Fu, L. Yang, Y. Ji, J. Xie and Z. Ding, *Coordin. Chem. Rev.*, 2026, **548**, 217157.
13 S. Feng, H. Hao Ngo, W. Guo, S. Woong Chang, D. Duc Nguyen, D. Cheng, S. Varjani, Z. Lei and Y. Liu, *Bioresour. Technol.*, 2021, **335**, 125278.
14 V. Karthik, P. Senthil Kumar, D.-V. N. Vo, P. Selvakumar, M. Gokulakrishnan, P. Keerthana, V. Audilakshmi and J. Jeyanthi, *Environ. Chem. Lett.*, 2021, **19**, 2331–2350.
15 R. A. Sheldon, A. Basso and D. Brady, *Chem. Soc. Rev.*, 2021, **50**, 5850–5862.
16 L. Wang, X. Du, Y. Li, Y. Bai, T. Tang, J. Wu, H. Liang and D. Gao, *Crit. Rev. Environ. Sci. Technol.*, 2023, **53**, 1684–1708.
17 Z. Guo, J. J. Richardson, B. Kong and K. Liang, *Sci. Adv.*, 2020, **6**, eaaz0330.
18 A. P. Côté, A. I. Benin, N. W. Ockwig, M. O'Keeffe, A. J. Matzger and O. M. Yaghi, *Science*, 2005, **310**, 1166–1170.
19 H. Furukawa, K. E. Cordova, M. O'Keeffe and O. M. Yaghi, *Science*, 2013, **341**, 1230444.
20 B. Wang, R.-B. Lin, Z. Zhang, S. Xiang and B. Chen, *J. Am. Chem. Soc.*, 2020, **142**, 14399–14416.
21 Y. Feng, Y. Xu, S. Liu, D. Wu, Z. Su, G. Chen, J. Liu and G. Li, *Coord. Chem. Rev.*, 2022, **459**, 214414.
22 S. Huang, G. Chen and G. Ouyang, *Chem. Soc. Rev.*, 2022, **51**, 6824–6863.
23 C. Doonan, R. Riccò, K. Liang, D. Bradshaw and P. Falcaro, *Acc. Chem. Res.*, 2017, **50**, 1423–1432.
24 X. Liu, M. Qiu, Y. Zhang, J. Pan, W. Zhang, L. Guo, X. Zhang and Y. Jiang, *Adv. Colloid Interface Sci.*, 2025, **344**, 103589.
25 M. Feng, C. Xing, Y. Jin, X. Feng, Y. Zhang and B. Wang, *J. Am. Chem. Soc.*, 2024, **146**, 32883–32905.
26 H. Wang, X. Kou, R. Gao, S. Huang, G. Chen and G. Ouyang, *Environ. Sci. Technol.*, 2024, **58**, 11869–11886.
27 L. Tong, S. Huang, G. Chen and G. Ouyang, *Angew. Chem., Int. Ed.*, 2025, **64**, e202421192.
28 W. Huang, H. Yuan, H. Yang, X. Ma, S. Huang, H. Zhang, S. Huang, G. Chen and G. Ouyang, *Nat. Commun.*, 2023, **14**, 3644.
29 R. Gao, X. Kou, L. Tong, Z. W. Li, Y. Shen, R. He, L. Guo, H. Wang, X. Ma, S. Huang, G. Chen and G. Ouyang, *Angew. Chem., Int. Ed.*, 2024, **63**, e202319876.
30 W. Tan, T. Wei, J. Huo, M. Loubidi, T. Liu, Y. Liang and L. Deng, *ACS Appl. Mater. Interfaces*, 2019, **11**, 36782–36788.
31 R. J. Drout, L. Robison and O. K. Farha, *Coord. Chem. Rev.*, 2019, **381**, 151–160.
32 X. G. Yang, J. R. Zhang, X. K. Tian, J. H. Qin, X. Y. Zhang and L. F. Ma, *Angew. Chem., Int. Ed.*, 2023, **62**, e202216699.
33 F. L. Oliveira, S. P. de Souza, J. Bassut, H. M. Álvarez, Y. Garcia-Basabe, R. O. M. Alves de Souza, P. M. Esteves and R. S. B. Gonçalves, *Chem. – Eur. J.*, 2019, **25**, 15863–15870.
34 Y. Lu, X. Wu, H. Lou and Z. Li, *Langmuir*, 2025, **41**, 11765–11775.
35 Q. Sun, C.-W. Fu, B. Aguila, J. Perman, S. Wang, H.-Y. Huang, F.-S. Xiao and S. Ma, *J. Am. Chem. Soc.*, 2018, **140**, 984–992.
36 C. Wang and K. Liao, *ACS Appl. Mater. Interfaces*, 2021, **13**, 56752–56776.
37 R. Gao, X. Kou, S. Huang, G. Chen and G. Ouyang, *ChemBioChem*, 2024, **25**, e202400339.
38 V. Lykourinou, Y. Chen, X.-S. Wang, L. Meng, T. Hoang, L.-J. Ming, R. L. Musselman and S. Ma, *J. Am. Chem. Soc.*, 2011, **133**, 10382–10385.
39 P. Li, Q. Chen, T. C. Wang, N. A. Vermeulen, B. L. Mehdi, A. Dohnalkova, N. D. Browning, D. Shen, R. Anderson, D. A. Gómez-Gualdrón, F. M. Cetin, J. Jagiello, A. M. Asiri, J. F. Stoddart and O. K. Farha, *Chem*, 2018, **4**, 1022–1034.
40 L. Guo, R. He, G. Chen, H. Yang, X. Kou, W. Huang, R. Gao, S. Huang, S. Huang, F. Zhu and G. Ouyang, *J. Am. Chem. Soc.*, 2024, **146**, 17189–17200.
41 S. Liang, X.-L. Wu, J. Xiong, M.-H. Zong and W.-Y. Lou, *Coord. Chem. Rev.*, 2020, **406**, 213149.
42 Y. Liu, J. Wang, X. Qin, G. Liu and H. Zhang, *Food Chem.*, 2025, **493**, 145602.
43 G. Chen, S. Huang, Y. Shen, X. Kou, X. Ma, S. Huang, Q. Tong, K. Ma, W. Chen, P. Wang, J. Shen, F. Zhu and G. Ouyang, *Chem*, 2021, **7**, 2722–2742.
44 X. Li, D. Li, Y. Zhang, P. Lv, Q. Feng and Q. Wei, *Nano Energy*, 2020, **68**, 104308.
45 R. Xu, M. Liu, C. Yao and X. Xu, *ACS Appl. Mater. Interfaces*, 2025, **17**, 5401–5409.
46 J. Liang, Z. Huang, K. Wang, L. Zhang, Y. Wan, T. Yang and H. Zeng, *Talanta*, 2023, **259**, 124503.
47 X. Cao, Y. Guo, M. Zhao, J. Li, C. Wang, J. Xia, T. Zou and Z. Wang, *Food Chem.*, 2022, **381**, 132282.
48 D. Chen, L. Wang, J. Wei, T. Jiao, Q. Chen, M. Oyama, Q. Chen, X. Chen and X. Chen, *Food Chem.*, 2024, **442**, 138389.
49 J. Huang, L. Jiao, W. Xu, H. Wang, M. Sha, Z. Wu, W. Gu, L. Hu and C. Zhu, *J. Hazard. Mater.*, 2022, **432**, 128707.
50 H. Ma, M. Li, T. Yu, H. Zhang, M. Xiong and F. Li, *ACS Appl. Mater. Interfaces*, 2021, **13**, 44329–44338.
51 Y. Bai, S. Nie, W. Gao, N. Li, P. Zhu, L. Zhang and J. Yu, *Adv. Funct. Mater.*, 2024, **35**, 2419499.
52 J. Mehta, S. Dhaka, N. Bhardwaj, A. K. Paul, S. Dayananda, S.-E. Lee, K.-H. Kim and A. Deep, *Sens. Actuators, B*, 2019, **290**, 267–274.
53 H. Li, Q. Lu, J. Shi, X. Zhang, P. Sun, X. Yan and G. Lu, *Adv. Funct. Mater.*, 2023, **34**, 2309383.
54 M. Li, S. Qiao, Y. Zheng, Y. H. Andaloussi, X. Li, Z. Zhang, A. Li, P. Cheng, S. Ma and Y. Chen, *J. Am. Chem. Soc.*, 2020, **142**, 6675–6681.
55 Y. Zheng, S. Zhang, J. Guo, R. Shi, J. Yu, K. Li, N. Li, Z. Zhang and Y. Chen, *Angew. Chem., Int. Ed.*, 2022, **61**, e202208744.
56 R. Gao, N. Zhong, L. Tong, X. Kou, W. Huang, H. Yang, S. Huang, J. Wu, G. Chen and G. Ouyang, *Cell Rep. Phys. Sci.*, 2022, **3**, 101153.
57 J. Chen, Z. Guo, Y. Xin, Z. Gu, L. Zhang and X. Guo, *Sci. Total Environ.*, 2023, **867**, 161510.
58 Y. Chen, K. Yu, M. Hassan, C. Xu, B. Zhang, K. Y.-H. Gin and Y. He, *Ecotoxicol. Environ. Saf.*, 2018, **166**, 320–327.
59 H. Patel, D. Rawtani and Y. K. Agrawal, *Trends Food Sci. Tech.*, 2019, **85**, 78–91.
60 D.-M. Liu, B. Xu and C. Dong, *TrAC, Trends Anal. Chem.*, 2021, **142**, 116320.
61 C. Jin, S. Yang, J. Zheng, F. Chai and M. Tian, *Food Chem.*, 2024, **459**, 140369.
62 X. Wang, S. Yang, J. Shan and X. Bai, *Int. J. Electrochem. Sci.*, 2022, **17**, 220543.
63 H. Liang, L. Wang, Y. Yang, Y. Song and L. Wang, *Biosens. Bioelectron.*, 2021, **193**, 113553.
64 H. Chai, Y. Li, K. Yu, Z. Yuan, J. Guan, W. Tan, J. Ma, X. Zhang and G. Zhang, *Anal. Chem.*, 2023, **95**, 16383–16391.
65 L. Wen, N. Wang, Z. Liu, C.-A. Tao, X. Zou, F. Wang and J. Wang, *Chemosensors*, 2022, **10**, 418.
66 Y. Luo, N. Wu, L. Wang, Y. Song, Y. Du and G. Ma, *Biosensors*, 2022, **12**, 625.
67 Y. Xiao, N. Wu, L. Wang and L. Chen, *Biosensors*, 2022, **12**, 899.
68 Q. Wu, Y. Wang, L. Wang, Y. Su, G. He, X. Chen, L. Hou, W. Zhang and Y. Y. Wang, *ACS Appl. Mater. Interfaces*, 2024, **16**, 55802–55812.
69 S. Dong, L. Peng, W. Wei and T. Huang, *ACS Appl. Mater. Interfaces*, 2018, **10**, 14665–14672.
70 C. Gong, D. Wang and H. Zhao, *Small*, 2023, **19**, e2304077.
71 C. Gong, B. Chen, Y. Xing and H. Zhao, *J. Hazard. Mater.*, 2024, **463**, 132849.
72 K. Yang, H. Zhao, N. Li, Y. Wang, B. Sun, M. Cui and C. Zhang, *Microchem. J.*, 2024, **203**, 110945.

73 Y. Liu, M. Zhou, C. Jin, J. Zeng, C. Huang, Q. Song and Y. Song, *Front. Chem.*, 2020, **8**, 643.
74 K. Niu, Y. Zhang, J. Chen and X. Lu, *ACS Sens.*, 2022, **7**, 3551–3559.
75 K. Niu, P. Sun, J. Chen and X. Lu, *Anal. Chem.*, 2022, **94**, 17177–17185.
76 Y. Zhao, X. Lu and F. Gao, *Anal. Biochem.*, 2022, **646**, 114628.
77 W. Wei, S. Zhou, D. D. Ma, Q. Li, M. Ran, X. Li, X. T. Wu and Q. L. Zhu, *Adv. Funct. Mater.*, 2023, **33**, 2302917.
78 H. Zhao, X. Tan, H. Chai, L. Hu, H. Li, L. Qu, X. Zhang and G. Zhang, *Chin. Chem. Lett.*, 2025, **36**, 110571.
79 E. Xie, Z. Chen, X. Zhang, X. Zhang, L. Zheng, X. Wang and D. Zhang, *J. Hazard. Mater.*, 2025, **492**, 138159.
80 J. Mehta, S. Dhaka, A. K. Paul, S. Dayananda and A. Deep, *Environ. Res.*, 2019, **174**, 46–53.
81 Z. Wang, B. Ma, C. Shen and L.-Z. Cheong, *Talanta*, 2019, **197**, 356–362.
82 B. Ma, L.-Z. Cheong, X. Weng, C.-P. Tan and C. Shen, *Electrochim. Acta*, 2018, **283**, 509–516.
83 C. Liu, X. Wang, X. Jia, W. He, S. Zhang and H. Liu, *Chem. Eng. J.*, 2025, **520**, 166170.
84 M. Romero-Lopez, M. Oria, F. Ferrer-Marquez, M. F. Varela, K. Lampe, M. Watanabe-Chailland, L. Martinez and J. L. Peiro, *Pediatr. Surg. Int.*, 2023, **39**, 180.
85 Y. Cheng, O. M. Lai, C. P. Tan, W. Panpipat, L. Z. Cheong and C. Shen, *ACS Appl. Mater. Interfaces*, 2021, **13**, 4146–4155.
86 Y. Cheng, B. Ma, C.-P. Tan, O.-M. Lai, W. Panpipat, L.-Z. Cheong and C. Shen, *Sens. Actuators, B*, 2020, **321**, 128477.
87 Y. Chen, G. Yuan, L. Tan, P. Wang, R. Lu and C. Wang, *J. Inorg. Organomet. Polym. Mater.*, 2022, **32**, 4401–4411.
88 Y. Ma and Y. Li, *Microchim. Acta*, 2023, **190**, 492.
89 R.-I. Stefan-van Staden, R. G. Bokretsion, J. F. van Staden and H. Y. Aboul-Enein, *Crit. Rev. Anal. Chem.*, 2015, **45**, 2–31.
90 X. Yan, C. Wei, C. Su, X. Liu, P. Sun, Z. Xu, G. Lu, Y. Lin and H. Li, *Adv. Funct. Mater.*, 2025, **35**, 2420159.
91 D. Su, T. Wang, A. Li, Y. Ma, X. Liu, C. Wang, X. Jia, P. Sun, F. Liu, X. Yan and G. Lu, *Adv. Funct. Mater.*, 2022, **32**, 2204130.
92 X. Yan, D. Su, H. Li, X. Zhao, X. Liu, F. Liu, P. Sun and G. Lu, *Adv. Funct. Mater.*, 2023, **33**, 2215192.
93 G. Chen, W. Xu, W. Gu and C. Zhu, *Anal. Chem.*, 2025, **97**, 16019–16025.
94 Y. Yin, C. Gao, Q. Xiao, G. Lin, Z. Lin, Z. Cai and H. Yang, *ACS Appl. Mater. Interfaces*, 2016, **8**, 29052–29061.
95 W. Sun, H. Chu, X. Zha, S. Lu and Y. Wang, *ACS Appl. Nano Mater.*, 2023, **6**, 15183–15192.
96 H. Liu, Y. Du, J. Gao, L. Zhou, Y. He, L. Ma, G. Liu, Z. Huang and Y. Jiang, *Ind. Eng. Chem. Res.*, 2019, **59**, 42–51.
97 J. Ma, J. Yuan, Y. Xu, Y. Jiang, W. Bai and J. Zheng, *Chem. Eng. J.*, 2022, **446**, 137001.
98 Y. Wen, R. Li, J. Liu, X. Zhang, P. Wang, X. Zhang, B. Zhou, H. Li, J. Wang, Z. Li and B. Sun, *Anal. Chim. Acta*, 2020, **1127**, 131–139.
99 D. Li, Y. Cheng, H. Zuo, W. Zhang, G. Pan, Y. Fu and Q. Wei, *J. Colloid Interface Sci.*, 2021, **603**, 771–782.
100 X. Zhong, F. Wang, J. Piao and Y. Chen, *Analyst*, 2021, **146**, 2825–2833.
101 L. Wang, G. Liu, Y. Ren, Y. Feng, X. Zhao, Y. Zhu, M. Chen, F. Zhu, Q. Liu and X. Chen, *Anal. Chem.*, 2020, **92**, 14259–14266.
102 Y. Dong, N. Feng, P. Liu, Q. Wei, X. Peng, F. Jiang and Y. Chen, *Small*, 2024, **20**, e2309075.
103 L. Gao, J. Wen, Z. Huang, S. Sheng, F. Xu, G. Ma and H. Tan, *ACS Appl. Mater. Interfaces*, 2023, **15**, 31224–31232.
104 S. Li, H. Xie, F. Xie, Q. Yi and H. Tan, *Microchim. Acta*, 2022, **189**, 358.
105 C. Zhang, Y. Wang, Y. Sun, J. Duan, M. Wang, S. Ai and J. Hou, *Sens. Actuators, B*, 2022, **369**, 132362.
106 D. K. Dey, J. I. Kang, V. K. Bajpai, K. Kim, H. Lee, S. Sonwal, J. Simal-Gandara, J. Xiao, S. Ali, Y. S. Huh, Y.-K. Han and S. Shukla, *Crit. Rev. Food Sci. Nutr.*, 2023, **63**, 8489–8510.
107 B. Wang, Y. Chen, Y. Wu, B. Weng, Y. Liu, Z. Lu, C. M. Li and C. Yu, *Biosens. Bioelectron.*, 2016, **78**, 23–30.
108 F. Hong, L. Ren and Y. Chen, *Chem. Eng. J.*, 2023, **452**, 139149.
109 L. Ren, F. Hong, L. Zeng and Y. Chen, *ACS Appl. Mater. Interfaces*, 2022, **14**, 51234–51243.
110 X. Xu, Z. Luo, K. Ye, X. Zou, X. Niu and J. Pan, *J. Hazard. Mater.*, 2021, **412**, 124407.
111 S. Wang, V. Rohani, P. Leroux, C. Gracian, V. Nastasi and L. Fulcheri, *Chemosphere*, 2024, **364**, 143174.
112 Y. Xu, H. Yang, A. Huang, L. Tong, W. Huang, G. Chen, W. Yi, S. Huang and G. Ouyang, *Chem. Sci.*, 2024, **15**, 19609–19618.
113 Y. Tong, J. Yang, F. Xia and J. Gu, *JACS Au*, 2025, **5**, 178–186.
114 J. Guo, X. Yue, Y. Hou, Y. Wang, Y. Liu, G. Liu, Y. He, L. Ma, L. Zhou and Y. Jiang, *Int. J. Biol. Macromol.*, 2024, **278**, 134641.
115 J. Song, W. He, H. Shen, Z. Zhou, M. Li, P. Su and Y. Yang, *Chem. Eng. J.*, 2019, **363**, 174–182.
116 J.-C. Lee, S. Y. Kim, J. Song, H. Jang, M. Kim, H. Kim, S. Q. Choi, S. Kim, P. Jolly, T. Kang, S. Park and D. E. Ingber, *Nat. Commun.*, 2024, **15**, 711.
117 L. Zhou, R. Yang, X. Li, N. Dong, B. Zhu, J. Wang, X. Lin and B. Su, *J. Am. Chem. Soc.*, 2023, **145**, 23727–23738.
118 W. Zhan, C. Wang, X. Yang, H. Li, S. Xiong and X. Li, *Environ. Int.*, 2024, **186**, 108598.
119 Q. Luo, X. Yan, J. Lu and Q. Huang, *Environ. Sci. Technol.*, 2018, **52**, 10617–10626.
120 S. Li, X. Chen, Q. Tian, J. Liu, Z. Tang and X. Niu, *Anal. Chem.*, 2025, **97**, 2537–2545.
121 T. Tian, D. Song, L. Zhen, Z. Bi, L. Zhang, H. Huang and Y. Li, *Biosens. Bioelectron.*, 2025, **277**, 117286.
122 Y. Li, F. Chen, Y. Liu, M. A. Khan, H. Zhao, H. Cao and D. Ye, *Chem. Eng. J.*, 2025, **511**, 162115.
123 H. Ibrahim, S. Moru, P. Schnable and L. Dong, *ACS Sens.*, 2022, **7**, 2293–2302.
124 M. H. Wong, J. P. Giraldo, S.-Y. Kwak, V. B. Koman, R. Sinclair, T. T. S. Lew, G. Bisker, P. Liu and M. S. Strano, *Nat. Mater.*, 2017, **16**, 264–272.
125 A. Tricoli, A. R. D. Lowe and T. Tsuzuki, *Chem. Eng. J.*, 2021, **413**, 127511.
126 X. Luo, Z. Fang, K. Ren, H. Zou and Q. Liu, *Environ. Sci. Technol.*, 2026, **60**, 4658.